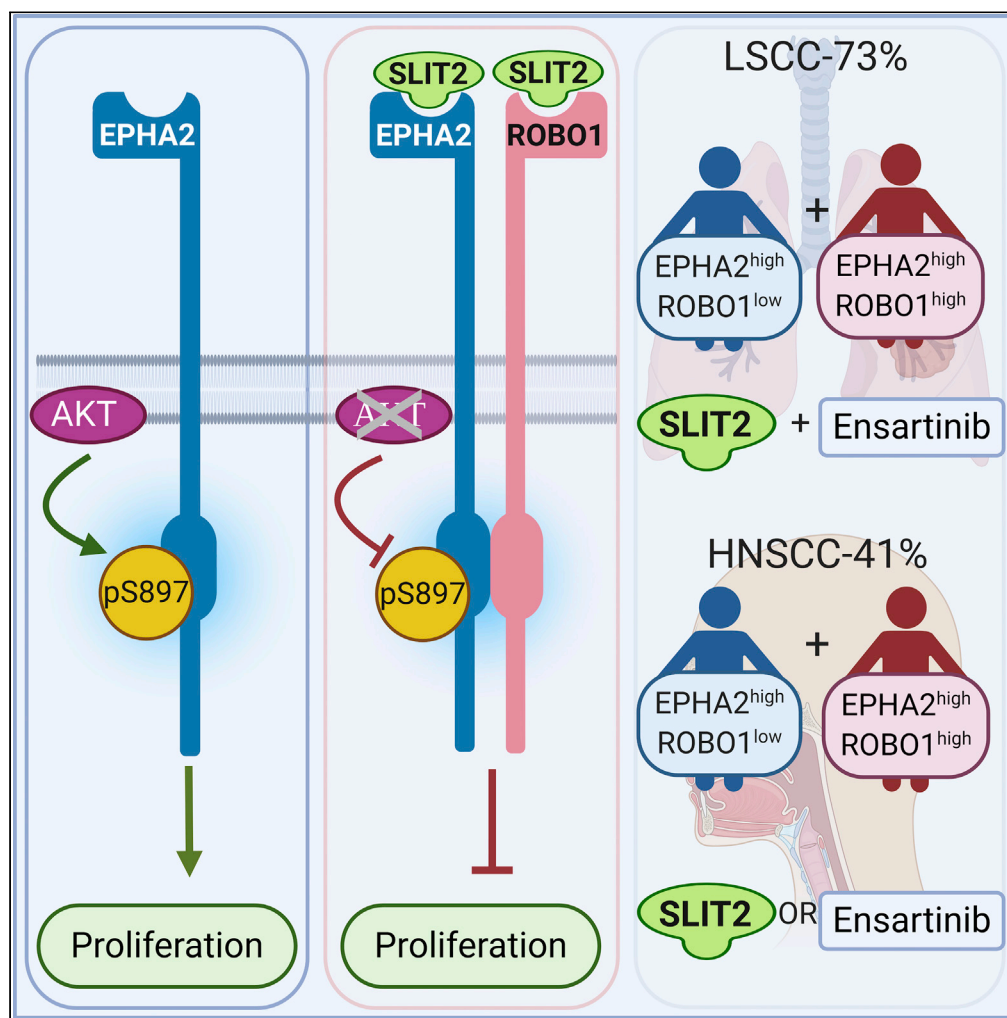**Article**

Activation of EPHA2-ROBO1 Heterodimer by SLIT2 Attenuates Non-canonical Signaling and Proliferation in Squamous Cell Carcinomas

Saumya Srivastava, Ka Ming Pang, Mari Iida, ..., Prakash Kulkarni, Deric L. Wheeler, Ravi Salgia

dlwheeler@wisc.edu (D.L.W.)
rsalgia@coh.org (R.S.)

HIGHLIGHTS

EPHA2 heterodimerizes with ROBO1 in LSCC and HNSCC

SLIT2 inhibits non-canonical signaling and cellular proliferation in SCCs

SLIT2 is a potential therapeutic and EPHA2 and ROBO1 are potential theranostics

iScience

Article

Activation of EPHA2-ROBO1 Heterodimer by SLIT2 Attenuates Non-canonical Signaling and Proliferation in Squamous Cell Carcinomas

Saumya Srivastava,[1,6] Ka Ming Pang,[2,6] Mari Iida,[3,6] Michael S. Nelson,[4] Jiayi Liu,[1,7] Arin Nam,[1] Jiale Wang,[1,8] Isa Mambetsariev,[1] Raju Pillai,[5] Atish Mohanty,[1] Nellie McDaniel,[3] Amita Behal,[1] Prakash Kulkarni,[1] Deric L. Wheeler,[3,*] and Ravi Salgia[1,9,*]

SUMMARY

The tyrosine kinase receptor ephrin receptor A2 (EPHA2) is overexpressed in lung (LSCC) and head and neck (HNSCC) squamous cell carcinomas. Although EPHA2 can inhibit tumorigenesis in a ligand-dependent fashion via phosphorylation of Y588 and Y772, it can promote tumorigenesis in a ligand-independent manner via phosphorylation of S897. Here, we show that EPHA2 and Roundabout Guidance Receptor 1 (ROBO1) interact to form a functional heterodimer. Furthermore, we show that the ROBO1 ligand Slit Guidance Ligand 2 (SLIT2) and ensartinib, an inhibitor of EPHA2, can attenuate growth of HNSCC cells and act synergistically in LSCC cells. Our results suggest that patients with LSCC and HNSCC may be stratified and treated based on their EPHA2 and ROBO1 expression patterns. Although ~73% of patients with LSCC could benefit from SLIT2+ensartinib treatment, ~41% of patients with HNSCC could be treated with either SLIT2 or ensartinib. Thus, EPHA2 and ROBO1 represent potential LSCC and HNSCC theranostics.

INTRODUCTION

With an estimated 2.09 million new cases that account for >13% of total cancer diagnoses, and 1.76 million deaths in 2018, lung cancer is the most common cancer and a leading cause of cancer-related deaths worldwide (Adjei, 2019). Non-small cell lung cancer (NSCLC) represents ~85% of all lung cancers with the majority of patients presenting with advanced stages of the disease when diagnosed. Squamous cell carcinoma of the lung (LSCC) is the second most common histology in NSCLC accounting for 20%–30% of all NSCLC cases and, more often than not, it presents with advanced stage disease at diagnosis (Herbst et al., 2018). Head and neck cancers represent the sixth most common cancer worldwide and accounts for approximately 650,000 new cases and more than 350,000 deaths every year. In the United States, head and neck cancer accounts for 3% of all cancers, with an estimated 53,000 Americans developing head and neck cancer annually and 10,800 dying from the disease. Approximately 90% of head and neck cancers are squamous cell carcinomas (HNSCCs) that arise from the mucosal surfaces of the oral cavity, oropharynx, and larynx. Tobacco use, alcohol consumption, Epstein-Barr virus infection, and HPV infection are some of the risk factors that are known to contribute to the development of almost 80% of the HNSCC cases diagnosed globally (Bray et al., 2018; Siegel et al., 2020). However, there are limited treatment options for advanced SCC, both in first-line and relapsed/refractory settings. In the last few years, several new drugs that include an anti-EGFR monoclonal antibody (necitumumab) in combination with standard chemotherapy and immune-checkpoint inhibitors such as nivolumab, pembrolizumab, or atezolizumab have been approved for treating SCC. Although the initial response to these drugs is encouraging, the patients eventually acquire resistance during the course of treatment, emphasizing the need for new drug targets and more efficacious drugs (Zappa and Mousa, 2016; Sabari and Paik, 2017).

The ephrin receptors (EPHR) and their ligands, the ephrins, play critical roles in a broad range of biological processes including neuronal pathfinding, angiogenesis, T cell activation, and stem cell maintenance (Darling and Lamb, 2019; Mosch et al., 2010). At the cellular level, the EPHR pathway regulates polarity, motility, proliferation, and survival in normal as well as neoplastic conditions (Singh et al., 2012; Lisabeth

[1]Department of Medical Oncology & Therapeutics Research, City of Hope National Medical Center, 1500 East Duarte Road, Duarte, CA 91010, USA

[2]Department of Surgery, City of Hope National Medical Center, Duarte, CA, USA

[3]Department of Human Oncology, University of Wisconsin School of Medicine and Public Health, Wisconsin Institute for Medical Research, Madison, WI 53705-2275, USA

[4]Light Microscopy Core, City of Hope National Medical Center, Duarte, CA, USA

[5]Department of Pathology, City of Hope National Medical Center, Duarte, CA, USA

[6]These authors contributed equally

[7]Present address: Shanghai Children's Medical Center, School of Medicine Shanghai Jiao Tong University, Shanghai, China.

[8]Present address: Shunde Hospital of Southern Medical University, Foshan, Guangdong, China.

[9]Lead Contact

*Correspondence: dlwheeler@wisc.edu (D.L.W.), rsalgia@coh.org (R.S.) https://doi.org/10.1016/j.isci.2020.101692

et al., 2013). In humans, ephrins and ephrin receptors constitute the largest receptor tyrosine kinase (RTK) family with a total of 14 members. Upregulation of EPH receptors, particularly EPHA2 and EPHB4, has been broadly implicated in the growth and metastasis of solid tumors, including NSCLC (Zelinski et al., 2001; Fang et al., 2005; Faoro et al., 2010; Ferguson et al., 2013; Pasquale, 2010; Salgia and Kulkarni, 2018; Tan et al., 2019). High levels of EPHA2 have been correlated with brain metastasis, disease relapse, and overall poor patient survival in lung cancers (Amato et al., 2014). In addition, EPHA2 is involved in acquired resistance to EGFR tyrosine kinase inhibitors (TKIs) and anti-EGFR antibodies (Zhuang et al., 2010; Koch et al., 2015; Amato et al., 2016), further highlighting the role of EPHA2 in tumor progression.

Ephrins are classified into either class A or B depending upon how they bind to the cell membrane. Class A ephrins (ephrin A1 to A5) are tethered to the cell membrane via a glycosyl-phosphatidylinositol (GPI) anchor, whereas class B ephrins (ephrin B1 to B3) are integral membrane proteins that contain a single transmembrane domain. EPH receptors are classified according to the class of ligand they bind to. There are eight class A receptors (EPHA1 to A8) and six class B receptors (EPHB1 to B6) (Pasquale, 2010). Both the ligands and the receptors are membrane bound and typically elicit signaling through cell-cell contact that leads to clustering of the ligand-receptor complexes. In addition, the binding of the ligand to the receptor triggers downstream events in the ligand-bearing cells, referred to as reverse signaling (Pasquale, 2010; Salgia and Kulkarni, 2018; Boyd et al., 2014). Among the EPHRs, EPHA2 has been shown to possess both ligand-dependent as well as ligand-independent activities (Miao et al., 2009; Taddei et al., 2009). Although ligand-mediated activation of EPHA2 was shown to inhibit cell motility, the ligand-independent activities enhance invasiveness and viability and are linked to tumor progression (Miao et al., 2009; Beauchamp and Debinski, 2012; Brantley-Sieders, 2012; Zhou and Sakurai, 2017). Importantly, S897 phosphorylation by AKT or RSK is a key mediator of the ligand-independent activities (Miao et al., 2009; Zhou et al., 2015) leading to tumorigenesis. In C. elegans, the ortholog of the human ephrin receptor, VAB-1, and its ligand, ephrin, EFN-1, function as cues in neuroblasts for proper neuronal pathfinding and in epidermal movements during embryogenesis. Mutants of the VAB-1 and ephrin exhibit variable degree of defects in embryonic arrest, larval arrest, and morphogenesis with a high percentage of animals showing the notch head phenotype (George et al., 1998; Chin-Sang et al., 1999). The ephrin/VAB-1 pathway interacts genetically with the conserved axon guidance receptor SAX-3/ROBO pathway in a dose-dependent fashion and showed synthetic embryonic lethal phenotype (Ghenea et al., 2005; Bernadskaya et al., 2012). SAX-3/ROBO null mutants display embryonic defects independent of VAB-1/EPHR mutants. Interestingly, double mutants of SLT-1, a ligand of SAX-3 (ROBO) and VAB-1, also show enhanced cell migration defects in comparison with VAB-1/EPHR or SLT-1 single mutants indicating cross talk between the two pathways. In addition, the tyrosine kinase domain of VAB-1 physically binds to the intracellular domain of SAX-3, specifically at the juxtamembrane region and the conserved cytoplasmic region 1 (CC1) (Ghenea et al., 2005).

Roundabout guidance receptors (ROBOs) and their ligands, SLITs (Slit Guidance Ligand 2), were first identified as important signaling molecules involved in the neuronal development in Drosophila (Rothberg et al., 1988; Kidd et al., 1999). Since then, this function in neuronal development has been found to be highly conserved in metazoans. In addition, new functions of the SLIT-ROBO pathway have been discovered in angiogenesis and in the development of the lung, mammary glands, and kidneys (Xian et al., 2001; Greishammer et al., 2004; Bedell et al., 2005; Strickland et al., 2006; Chen et al., 2010; Blockus and Chedotal, 2016; Ballard and Hinck, 2012). Recent studies have also implicated the SLIT-ROBO pathway in cancer progression and metastasis (Huang et al., 2015; Gara et al., 2015; Maiti et al., 2015). There are four ROBOs (ROBO 1–4) and three SLITs (SLIT 1–3) in mammals that can bind to different ROBO receptors with differing affinities. All ROBO receptors contain a single transmembrane domain with several weakly conserved cytoplasmic (CC) domains and no clear functionally defined domain in the cytoplasmic tail. Therefore, additional signaling molecules are probably involved in directing cellular activities (Hohenester, 2008; Gara et al., 2015; Maiti et al., 2015; Blockus and Chedotal, 2016). ROBO1 overexpression and mutations in lung cancer have been correlated with better patient outcome (Dallol et al., 2002; Maiti et al., 2015). Suppression of SLIT2 was associated with advanced pathological stage and a poor survival rate among patients with lung cancer (Gara et al., 2015).

Despite the correlation between expression levels of EPHA2, ROBO1, and SLIT2, and tumorigenesis and clinical outcome in patients with lung cancer, the translational potential of this clinical research has not been fully explored. Here, we have investigated the roles of EPHA2 and ROBO1 in SCCs of the lung and head and neck. Our results demonstrate that EPHA2 can physically interact by heterodimerizing with
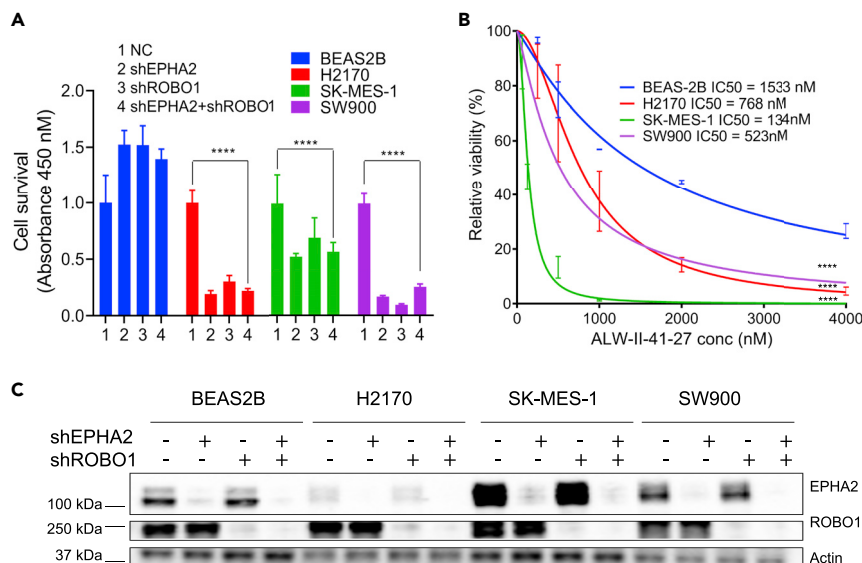
Figure 1. ROBO1 and EPHA2 Are Not Synthetic lethal in LSCC Cell Lines

shRNA-mediated knock down of EPHA2 and ROBO1 to study effect on cellular proliferation in lung cancer cell lines.

(A) Knockdown of EPHA2, ROBO1 and double knockdown via shRNA has variable effects on cellular proliferation among different cell lines in comparison with control cells BEAS-2B. We used four biological replicates and used two-way (ANOVA) to calculate the p values. shRNA knockdown for EPHA2, ROBO1 and double knockdown in H2170, SK-MES-1, and SW900 were significant p < 0.0001. But the double knockdown was not synthetic lethal in all cell lines. Data are represented as mean ± SD.

(B) Chemical ablation of EPHA2 using ALW-II-41-27 shows significant inhibition of proliferation in all lung cancer cell lines in comparison with control lung epithelial cells BEAS2B as indicated by values of IC50. The p values (p < 0.0001) are calculated using simple linear regression. Data are represented as mean ± SD.

(C) Immunoblot showing protein levels of EPHA2 and ROBO1 in single and double knockdowns compared with control. Related to Figure S1.

ROBO1 and this interaction is stabilized in the presence of SLIT2, which in turn attenuates cellular proliferation. Furthermore, the data also suggest that patients with LSCC and HNSCC may be stratified and treated based on their EPHA2 and ROBO1 expression patterns. Altogether our results indicate that SLIT2 is a potential therapeutic for LSCC and HNSCC and that EPHA2 and ROBO1 may represent potential theranostics in these two diseases.

RESULTS

ROBO1 and EPHA2 Are Not Synthetic Lethal in LSCC and HNSCC Cells

In *C. elegans*, double mutants of *sax-3* in the SLIT-ROBO and *vab-1* the ephrin-EPH pathway showed synthetic lethal phenotype in embryonic stage suggesting that there is cross talk between the two pathways (Ghenea et al., 2005). This interaction presents an attractive window of opportunity for developing targeted therapy against the EPH-ROBO pathway, if the underlying mechanism is conserved in SCC. Therefore, we first determined whether a knockdown or pharmacological inhibition of the EPH receptor (*vab-1*) in *C. elegans* exhibits a synthetic lethal phenotype with ROBO mutant (*sax-3*). Consistent with the phenotype of genetic double mutants, knocking down *vab-1* in *sax-3* or knocking down *sax-3* in *vab-1* mutants exhibited the synthetic lethal phenotype (Figures S1A–S1C). Figure S1C displays the percentage of F1 viable progeny that survived out of the total F1 population. Moreover, treating *sax-3* worms with ALW-II-41-27, a small molecule Eph family tyrosine kinase inhibitor, also enhanced lethality (Figure S1D), indicating that ALW-II-41-27 inhibited the ephrin receptor of *C. elegans* (Amato et al., 2014; Choi et al., 2009; Miao et al. 2015).

Next, to determine if EPHA2 is important for the survival of lung squamous cells, we knocked down EPHA2 using shRNA in three squamous cell carcinoma cell lines (H2170, SK-MES-1, and SW900) as well as in control, normal lung epithelial BEAS-2B cells and measured cell viability 96 h post transfection using the CCK8 cell survival assay. Although control BEAS-2B cells showed no growth inhibition, H2170 SK-MES-1 and

%Age Inhibition	BEAS2B	H2170	SK-MES-1	SW900
shEPHA2	−52.42	80.72	47.26	83.70
shROBO1	−52.01	69.58	30.35	90.90
shEPHA2+ROBO1	−39.55	77.89	42.88	75.02

Table 1. Percentage Inhibition of LSCC Cell Lines after shRNA Knockdown of EPHA2, ROBO1, and Double Knockdown

SW900 cells showed 80%, 47%, and 83% inhibition, respectively (Figure 1A). Similarly, treatment of cells with ALW-II-27-41 resulted in stronger inhibition of NSCLC cells (IC50 range from 134 to 768 nM) relative to control BEAS-2B cells (IC50 = 1,533 nM) (Figure 1B). These results support the idea that EPHA2 is involved in positive signaling for LSCC cell proliferation.

To further investigate the functional relationship between ROBO1 and EPHA2 in LSCC, we first determined whether ROBO1 knockdown also affects cell proliferation in various LSCC cell lines. Knocking down ROBO1 in H2170, SK-MES-1, and SW900 cells showed 69%, 30%, and 90% inhibition of proliferation, respectively (Figure 1A). We then asked if knocking down both EPHA2 and ROBO1 would show an enhancement of the inhibition shown in these cell lines. However, in all three cell lines, no additive effect was observed (Figure 1A and Table 1). To confirm the efficiency of shRNA knockdown, we determined the expression of EPHA2 and ROBO1 proteins by immunoblotting (Figure 1C). Next, a variety of head and neck cancer cell lines and cetuximab-resistant cell lines (HN30-C2, C4, and C5) expressing high EPHA2 were investigated (Figures 2A and 2D). Knockdown of either EPHA2 or ROBO1, or both (double knockdown), was performed using specific pooled siRNAs and the results were confirmed by immunoblotting (Figures 2B and 2E). When we performed the ROBO1 knockdown with siRNA in HNSCC cells and examined ROBO1 protein levels in the cell lysates by immunoblotting using Invitrogen antibody; we did not observe a decrease in the ROBO1 protein level. We repeated the immunoblot experiment with another antibody from Proteintech (Rosemont, IL, USA) that detects a smaller isoform and observed a complete knockdown of ROBO1. The Proteintech antibody was raised against a C-terminal fragment of human ROBO1 (residues 1,631-1,647), whereas the Invitrogen antibody was raised against a fragment corresponding to a region within amino acids 75 and 344 of Human ROBO1, which may explain the observed differences. However, we did not observe a significant effect on cell proliferation with EPHA2 or ROBO1 knockdown, or double knockdown (except for Tu138 and HN-30P cell lines), as determined by CCK-8 assay (Figures 2C and 2F).

These results support the idea that both EPHA2 and ROBO1 are involved in positive signaling for LSCC cell proliferation. The effect of shRNA knockdown of EPHA2 was less pronounced in SK-MES-1 cells. However, ALW-II-27-41 inhibited cell growth with an IC50 of 134 nm suggesting a role of other RTKs in these cells. Surprisingly, in spite of low levels of EPHA2 in H2170, shRNA knockdown of EPHA2 caused 80% inhibition of cell proliferation in these cells suggesting that EPHA2 is driving proliferation in these cells. We previously reported an activating EPHA2 mutation in its extracellular domain (G391A) in these cells that renders it constitutively active (Faoro et al., 2010). Thus, it is likely that low levels of the constitutively active receptor could have profound effects on cell growth via a ligand-independent mechanism. ALW-II-27-41 inhibited cell proliferation with lesser efficiency in H2170 compared with SW900 and SK-MES-1. In addition to EPHA2 and other RTKs that are sensitive to ALW-II-27-41, these cells may also have other pathways driving cell growth. SOX-2 is upregulated in LSCC cells H2170 but not in SK-MES-1 cells (Fukazawa et al., 2016). Therefore, it is possible that, in H2170 cells, SOX2 is driving tumorigenesis by suppressing CDKN1A (also called p21) that induces G1 cell-cycle arrest.

Since HNSCC cells are not dependent on EPHA2 and ROBO1 for cell growth because knocking down both proteins inhibited proliferation only 5%–10% except for Tu138 and HN-30P, it is possible that other RTK pathways may be involved. For example, we previously showed that AXL may be driving tumor growth in these cells (Brand et al., 2015).

Expression of EPHA2 and ROBO1 in LSCC and HNSCC Tissue Microarrays

Our previous studies with 105 NSCLC patient samples showed that EPHA2 was overexpressed in these patients (Faoro et al., 2010). Among the three types of lung cancer, LSCC specimens showed the highest
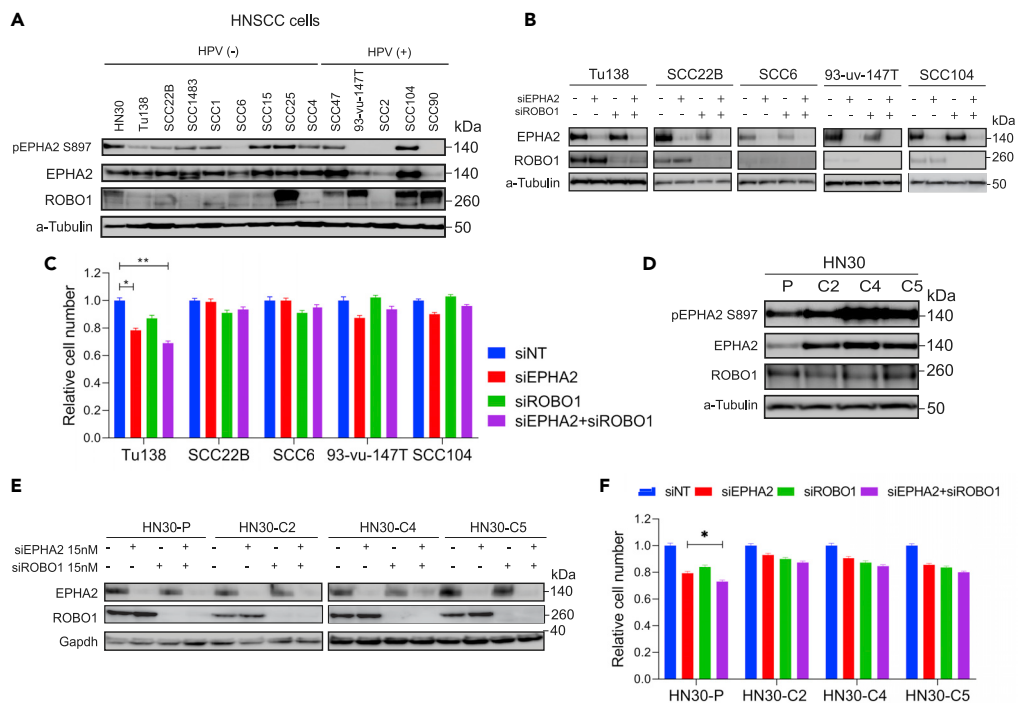
Figure 2. ROBO1 and EPHA2 Are Not Synthetic Lethal in HNSCC Cell Lines

EPHA2, ROBO1 and double siRNA-mediated knockdown to study effect on cellular proliferation.

(A) Levels of total EPHA2, ROBO1, and pEPHA2 S897 in head and neck cancer cell lines.

(B) Levels of EPHA2, ROBO1, and double knockdown confirming knockdown using siRNA.

(C) CCK8 assay to determine cellular proliferation inhibition after knocking down EPHA2, ROBO1, or both.

(D) Levels of total EPHA2, ROBO1, and pS897 in cetuximab-resistant cells.

(E) Levels of EPHA2 and ROBO1 after knocking down EPHA2, ROBO1, or both via siRNA.

(F) Relative cell number after CCK8 assay to determine cellular proliferation inhibition in EPHA2, ROBO1, and double knockdown in cetuximab-resistant cells. Data are represented as mean ± SD. P values calculated were found significant in Tu138 and HN-30P cell lines. P values were calculated using one-way (ANOVA). Related to Figure S1.

expression levels of EPHA2 (n = 24). To further correlate this trend, we examined EPHA2 expression using two tissue microarrays (TMAs), one with 64 LSCC samples and another with 60 HNSCC samples (Figures 3A and 3B). We categorized the TMA core into four categories based on EPHA2 and ROBO1 expression levels. EPHA2^{high}-ROBO1^{low}; EPHA2^{high}-ROBO1^{high}; EPHA2^{low}-ROBO1^{high}; EPHA2^{low}-ROBO1^{low}. The pathological scoring was interpreted by considering a score of +0, +1 as low expressing and +2 and +3 as high expressing. In LSCC, 73% (EPHA2^{high}-ROBO1^{low}) of the samples showed significant expression of EPHA2, whereas very few, ~2% (EPHA2^{low}-ROBO1^{high}) showed high expression levels of only ROBO1 and the remaining 25% showed low expression of both EPHA2 and ROBO1 (EPHA2^{low}-ROBO^{low}). A quantitative evaluation of the pathological scoring in LSCC TMA revealed that ROBO1 and EPHA2 exhibited an inverse relationship where most samples with high EPHA2 expression had low ROBO1 expression (Figures 3A and 3C). This correlates with the fact that higher ROBO1 levels are associated with better survival in patients with lung cancer since only a relatively small percentage of patients with lung cancer have good survival prognosis (Figures S2 and S3 and Table S1). On the other hand, in HNSCC, 12% samples show EPHA2^{high} and ROBO1^{low} expression, 29% showed EPHA2^{high} and ROBO1^{high} expression, and 17% showed EPHA2^{low} and ROBO1^{high} expression (Figures 3B and 3C). The remaining 42% were EPHA2^{high}-ROBO1^{low}. Based on the TMA results, we attempted to stratify patients with LSCC and HNSCC and observed a striking difference that may be helpful in determining the course of treatment of patients with squamous carcinoma LSCC and HNSCC (Figure 3C).

ROBO1 and SLIT2 Reside in the Same Complex and Physically Interact with EPHA2

To further probe the EPHA2/ROBO1 interaction, we used fluorescent proteins to tag ROBO1 and EPHA2 and tracked their localization using confocal microscopy. ROBO1-mCherry and EPHA2-mGFP were
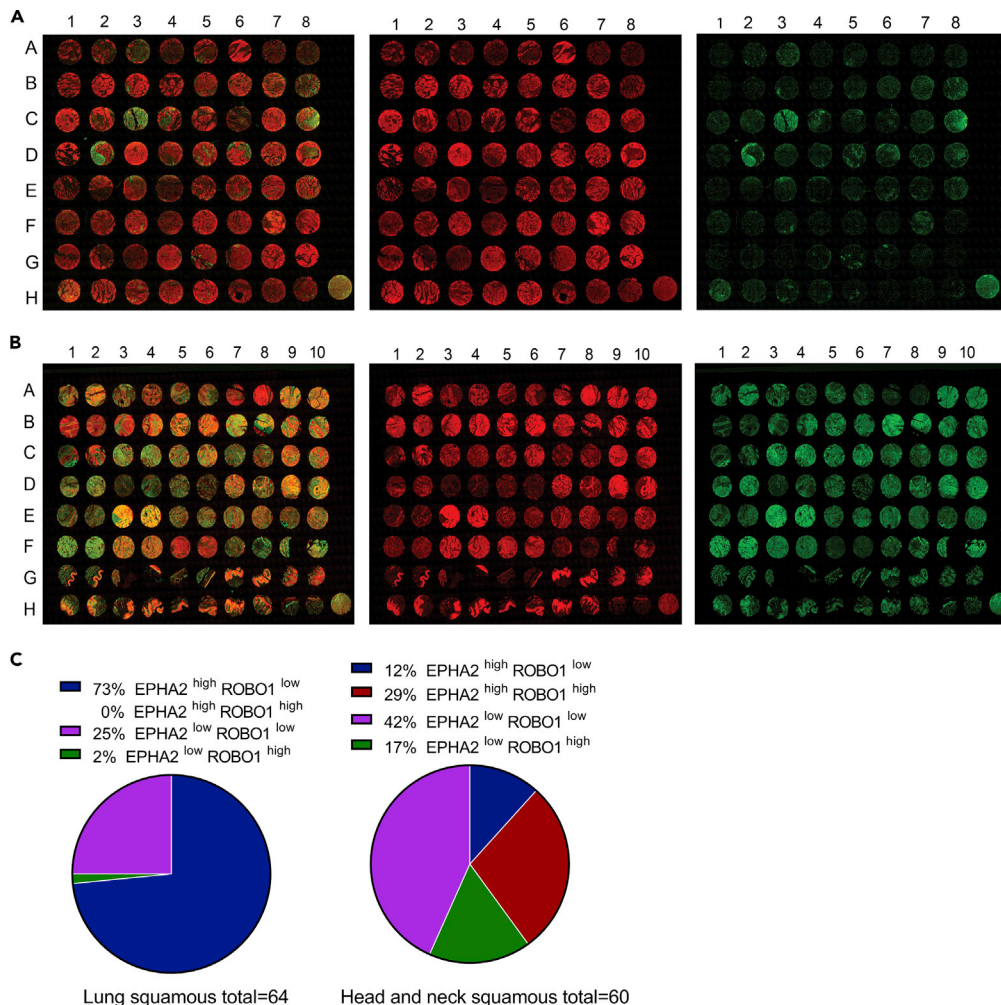
Figure 3. Expression of EPHA2 and ROBO1 Receptors in LSCC and HNSCC TMAs

(A) Sixty-four TMA panels of LSCC patient samples, TMA-LC642a purchased from Biomax. Pseudo colors show anti-EPHA2 (red) and anti-ROBO1 (green). The pseudo color was created by FIJI software.

(B) Sixty TMA panels of HNSCC patient samples, TMA-HN801B purchased from Biomax. Pseudo colors show anti-EPHA2 (red) and anti-ROBO1 (green).

(C) Pie-chart representing the quantification of pathologist scoring of LSCC and HNSCC TMAs (see Table S1). The images were taken at 20× magnification. Related to Figures S2 and S3.

localized to the cell surface as well as cytoplasmic vesicles (Figure 4A). The merged images showed that most of the EPHA2-mGFP and the ROBO1-mCherry co-localized at the cell membrane and in cytoplasmic vesicular structures. However, some discrete loci showed either EPHA2 or ROBO1 signal (Figure 4A). Z-section images revealed that both proteins localized in some discrete loci and in long extensions attached to surfaces (Figures 4A and Video S1). In addition, we also investigated the interaction between EPHA2 (Alexa Flour 547, red) and SLIT2 (Alexa Flour 488, green) in SW900 cells using confocal microscopy. We observed that EPHA2 and SLIT2 co-localized at the cell boundary and around nuclear membrane (Figure 4B).

Cytoplasmic and nuclear membrane staining have been observed in other studies too, that have used this EPHA2 antibody (Stammes et al., 2017). It is likely that EPHA2 translocates to the nucleus and has a role in transcription that has not been explored yet. It is also interesting to note that several other RTKs have been shown to be translocated to the nucleus (Xie et al., 2019). Translocation of MET to the nucleus promotes hepatocellular carcinoma tumorigeneses and metastasis by upregulation of TAK1 and activation of NF-κB pathway (Tey et al., 2017). MET has also been shown to regulate nuclear calcium (Gomes et al., 2008) and YAP signaling to stimulate cell proliferation or induce SOX9 and β-catenin to enhance ''cancer
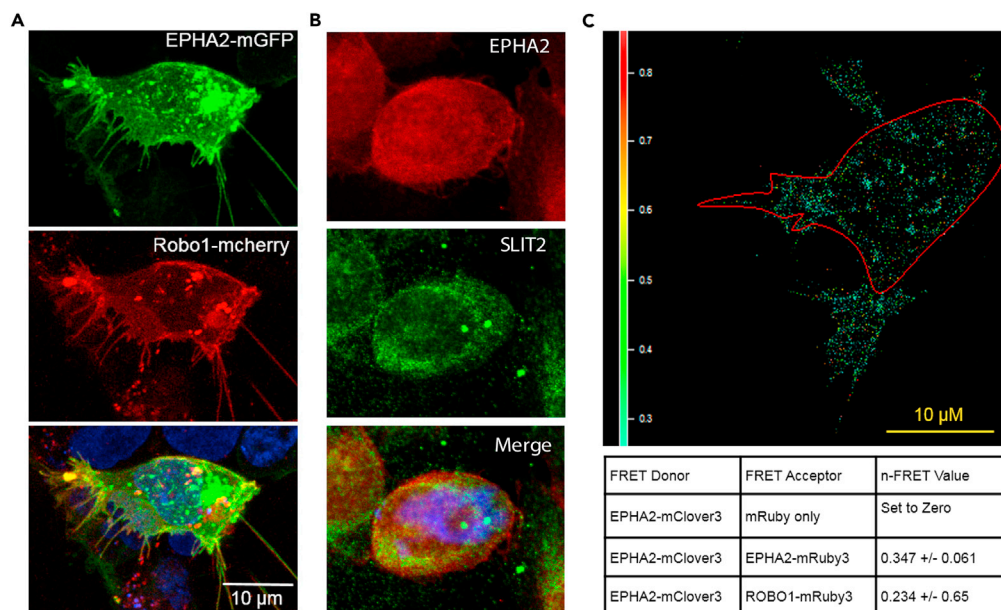
Figure 4. ROBO1/SLIT2 Are Present in the Same Complex and Physically Interact with EPHA2

EPHA2-ROBO1 and EPHA2-SLIT2 interaction in LSCC cells.

(A) EPHA2-GFP fusion (green) and ROBO1-m-cherry fusion (red) were co-expressed in cells for discerning interaction of EPHA2 and ROBO1 using confocal microscopy.

(B) Co-immunofluorescence of EPHA2 (Alexa Flour 547, red) and SLIT2 (Alexa Flour 488, green) in SW900 LSCC cells imaged with a confocal microscope. Yellow represents the area of co-expression of EPHA2 and SLIT2.

(C) FRET analysis. EPHA2-mClover3 was used as FRET donor and EPHA2-mRuby3, ROBO1-mRuby3 both were used as the FRET acceptors. EPHA2-mClover3 and EPHA2-mRuby3 were used as a positive control. FRET values are indicated. Images were taken at 40× magnification. Scale bar, 10 μm.

stem-like cells" self-renewal for cancer recurrence (Xie et al., 2014). Finally, complexes of the soluble forms of EPHA7 and EPHA10 were found to be localized in the cytoplasm as well as the nucleus in breast cancer cells (Johnson et al., 2016). These observations support the ability of EPHA2 to regulate gene expression, and its nuclear staining observed here suggests that it could putatively be involved in the regulation of transcription. Of note, EGFR has also been observed to translocate to the nucleus (Brand et al., 2011, 2013; Wang and Hung, 2009). A C-terminal fragment of ROBO1 has been reported to localize at the nucleus and promote tumorigenesis (Seki et al., 2010). SLIT2, on the other hand, has not been shown to localize to the nucleus but has been reported to inhibit transport of β-catenin to the nucleus (Chang et al., 2012).

To corroborate the interactions between EPHA2 and ROBO1, we used fluorescence resonance energy transfer (FRET) and confocal microscopy and determined the proximity of ROBO1 and EPHA2. For this purpose, we tagged ROBO1 with mClover3 (ROBO1-mClover3) as the FRET donor and EPHA2-mRuby3 (EPHA2-mRuby3) as the FRET acceptor. EPHA2-mClover3 and EPHA2-mRuby3 were used as a positive control; FRET was detected as expected with an N-FRET value of 0.347 ± 0.061. FRET was also detected between ROBO1-mClover3 and EPHA2-mRuby3 with N-FRET value of 0.234 +/0.065 (N = 23) (Figure 4C). Taken together, these data provided good evidence that EPHA2 and ROBO1 are in proximity (Foster radius of ~6 nm) to potentially make direct contact.

As additional evidence supporting interaction between EPHA2 and ROBO1, we performed co-immunoprecipitation (coIP) experiments. Plasmids constructs with FLAG-tagged ROBO-1 (ROBO1-FLAG) and HA tagged-EPHA2 (EPHA2- HA) were co-transfected into HEK293 cells, which express low endogenous levels of both EPHA2 and ROBO1. The LSCC cell lines were not used as the endogenous levels of ROBO1 in these cells are low to observe the interaction with EPHA2 using coIP. Indeed, in these experiments, EPHA2 protein was pulled down with ROBO1-FLAG tag IP (Figure 5A). To test if the kinase activity of EPHA2 is necessary for the interaction, we generated a kinase-dead (K645R) EPHA2-KD-HA construct (Taddei et al., 2009). Interestingly, a higher level of the kinase-dead mutant co-immunoprecipitated with ROBO1 than the wild-
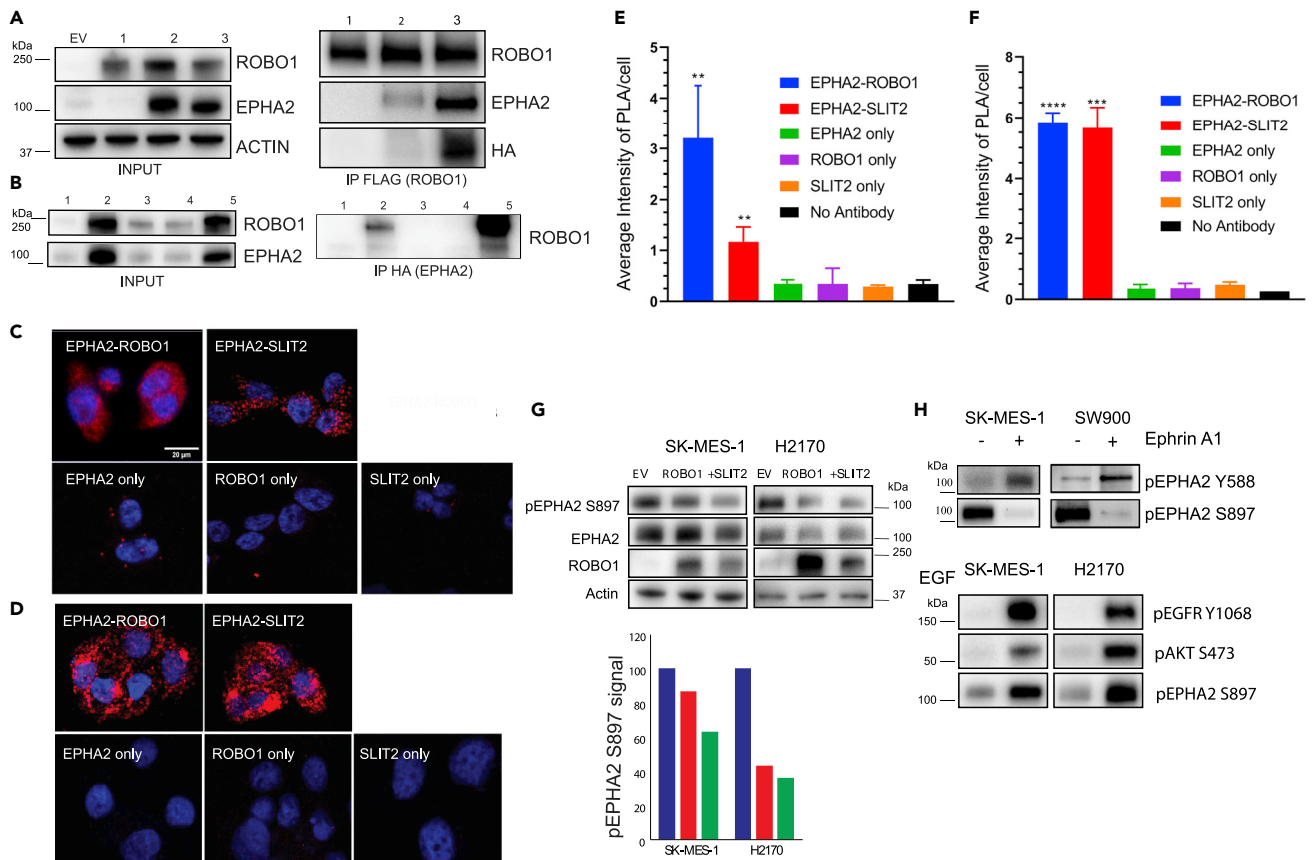
Figure 5. ROBO1/SLIT2 Interact with EPHA2 and Negatively Regulate Cell Proliferation

EPHA2 and ROBO1 reside in the same protein complex shown by biochemical assays. Co-immunoprecipitation assay for EPHA2 and ROBO1.

(A) Input and IP FLAG (ROBO1). EPHA2 wild-type and EPHA2 kinase dead EPHA2 (K645R KD) HA mutant is pulled down in complex with ROBO1. EV: Empty vector (mCherry FLAG); 1: ROBO1-FLAG; 2: ROBO1-FLAG + EPHA2-WT-HA; 3: ROBO1-FLAG + EPHA2-(K645R KD-HA).

(B) Input and Inverse IP HA of EPHA2 pulls down WT ROBO1 but the phosphorylation mutants of ROBO1 do not bind to EPHA2. EV: Empty vector (mCherry FLAG); 1: mCherry-FLAG + EPHA2-WT-HA; 2: ROBO1-FLAG + EPHA2-WT-HA; 3: ROBO1-FLAG Y932F + EPHA2-WT-HA; 4: ROBO1-FLAG Y1073F + EPHA2-WT-HA; 5: ROBO1-WT-FLAG + EPHA2- (K645R KD) HA.

(C) Proximity Ligation Assay. Interaction (protein-protein) of EPHA2-ROBO1 compared to EPHA2-SLIT2 in LSCC (SW900) cells represented by confocal images. The cell nucleus is stained with DAPI and the PLA is shown by red punctate staining. (E) Confocal microscopy images are quantified for red punctate staining representing the amount of PLA between the two proteins. (D) Proximity Ligation Assay. Interaction (protein-protein) of EPHA2-ROBO1 compared to EPHA2-SLIT2 in HNSCC (SCC1) cells represented by confocal images. The cell nucleus is stained with DAPI and the PLA is shown by red punctate staining. (F) Confocal microscopy images are quantified for red punctate staining representing the amount of PLA between the two proteins. Data are represented as mean $\pm$ SD. One-way (ANOVA) was performed to calculate p values. EPHA2-ROBO1 and EPHA2-SLIT2 interactions are significant in LSCC (p value < 0.001). The EPHA2-ROBO1 and EPHA2-SLIT2 both interactions are significant in HNSCC (p value < 0.0001). The images were taken at 40× magnification. Scale bar, 20 μm.

(G) ROBO1 was overexpressed in LSCC cell lines (SK-MES-1; H2170) and SLIT2 (2 μg/mL) was added to determine total EPHA2 and ROBO1 levels and pS897 levels. Densitometry of the bands of immunoblot in (G) normalized to band intensity of empty vector.

(H) SK-MES-1 and SW900 cells treated with ephrinA1 to discern canonical (pY588) and non-canonical signaling (pS897) hallmarks. EGF (0.5 μg/mL) was added to SK-MES-1 and H2170 cells to assay pS897 levels and pAKT (S473) and pEGFR (Y1068).

type EPHA2, even though the kinase-dead protein expressed at a lower level than the wild-type (Figure 5A) suggesting that the kinase activity of EPHA2 is not required for interaction between EPHA2 and ROBO1. Similarly, when we performed the corollary experiment and used HA tag IP for HA tagged-EPHA2, a higher level of WT ROBO1 was co-immunoprecipitated with the kinase dead EPHA2 than the wild-type EPHA2 (Figure 5B). Additionally, ROBO1 point mutations at Y932F, a ubiquitination site, and Y1073F, an ABL phosphorylation site, showed very low binding to WT-EPHA2 suggesting that these post-translational modifications may be important for interaction between EPHA2 and ROBO1. However, since the input protein of the ROBO1 phosphorylation mutants was low, additional experiments are needed to ascertain this

conjecture. Notwithstanding this caveat, these observations suggest that ROBO1 and EPHA2 reside in the same complex and interact with each other, but the interaction does not require EPHA2 kinase activity.

Finally, we ascertained that there is an interaction between EPHA2-ROBO1 and EPHA2 and SLIT2 ligand of ROBO1 by performing a proximity ligation assay (PLA) in both LSCC (SW900) and HNSCC (SCC1) cell lines. The results showed that EPHA2, ROBO1, and SLIT2 interact with each other in both the cell lines. However, HNSCC cells showed more robust interactions between EPHA2/ROBO1 and EPHA2/SLIT2 compared with LSCC cells (Figures 5C and 5D). The positive PLA signals were quantified using FIJI image software (Figures 5E and 5F). These results revealed that EPHA2 and ROBO1 can form a heterodimer and SLIT2 forms a complex with them. These interactions exert their effect on the tumor cells in both LSCC and HNSCC.

SLIT2/ROBO1 Interaction Negatively Regulates Cellular Proliferation and EPHA2 Tumorigenic Signaling

To assess the functional significance of the EPHA2/ROBO1 interaction, we examined the changes in EPHA2 signaling in LSCC cell lines in which ROBO1 was exogenously overexpressed. Upon binding to the ephrinA1, EPHA2 induces autophosphorylation of Y772 at the activation loop and Y588, Y594 at its juxtamembrane region, leading to the recruitment of downstream effectors (Fang et al., 2008; Pasquale, 2010; Boyd et al., 2014). Previous reports have also identified a ligand-independent activity of EPHA2 that is associated with phosphorylation at S897 by AKT and RSK (Miao et al., 2009; Zhou et al., 2015). Overexpression of ROBO1 in NSCLC cells resulted in down-regulation of pS897, the ligand-independent activity and tumorigenic marker of EPHA2. A more pronounced down-regulation of pS897 signal was observed when the cells (SK-MES-1 and H2170) were treated with SLIT2 (2 μg/mL for 72 h) (Figure 5G). When SK-MES-1 and SW900 cells were treated with ephrinA1 (2 μg/mL for 72 h), as expected, it enhanced ligand-dependent signaling via pY588 and suppressed tumorigenic signaling via pS897 (Figure 5H). Furthermore, addition of EGF (0.5 μg/mL for 72 h) to these cells not only activated EGF receptor and its downstream effectors like AKT but also enhanced the tumorigenic signature of pS897 (Figure 5H).

To assess the physiological changes in response to these ligands, we determined the effects of individual and combined treatments on cell proliferation and caspase activity. The cells were tagged with m-Kate2 (nuclear red fluorescence), and cell proliferation was monitored in real time using the IncuCyte Live Cell Analysis System (Sartorius, Bohemia, NY, USA). Caspase activity was monitored by using Caspase Green 3/7 substrate from IncuCyte, and the results indicated that SLIT2 and the EPHA2 inhibitors had a cytostatic effect in the majority of the instances (Table 3; Figures S4 and S5). The cells were treated with ephrin A1 at a concentration of 2 μg/mL but surprisingly, we did not see any inhibition of cell growth in both SW900 (LSCC) and SCC1 (HNSCC) cells (Figure S6E). In spite of seeing an increase in pY588 and a decrease in pS897 levels upon ephrin A1 treatment in LSCC cells, we do not observe any decrease in cell proliferation (Figures 5H and S6E). We previously demonstrated that the A859D mutation in EPHA2 causes the receptor to be activated in a ligand-independent fashion (Tan et al., 2019). Likewise, we also reported another mutation G391R in EPHA2 in LSCC that renders these cells insensitive to doxazosin an agonist of EPHA2 (Faoro et al., 2010) by affecting binding of the downstream effectors of EPHA2. Thus, it is likely that these cells do not respond to the ligand because they carry mutations in the EPHA2 receptor that makes them entirely independent of the ligand.

In SW900 LSCC cells with EPHA2^{high} and ROBO1^{low} expression (majority patient cases based on TMA scoring ~73%), treatment with SLIT2 resulted in 34% inhibition of cellular proliferation. This inhibition was rescued by sequential treatment with EGF (EGF was added 24 h following SLIT2 treatment) (Figure 6A, panel 1). Consistent with this finding, we observed that EGF leads to activation of pS897 of EPHA2 via AKT (Figure 5H). Inhibition of cellular growth was also observed with the EPHA2 inhibitor ALW-II-41-27 (54%), and the combination treatment with SLIT2 showed 61% inhibition (Figure 6B, panel 2). We also observed this effect with another EPHA2 inhibitor ensartinib (Horn et al., 2018) where it showed 41% inhibition by itself and when combined with SLIT2, showed 65% inhibition (Figure 6A, panel 3, Tables 2 and 4) suggesting that combination treatment would be beneficial for LSCC patients with EPHA2^{high} and ROBO1^{low} levels. To confirm this observation, we also tested another EPHA2^{high} and ROBO1^{low} cell line, SK-MES-1. We observed a significant inhibition with SLIT2 treatment and synergy in SK-MES-1 cells when combined with EPHA2 inhibitors (Figures 6B and Table 2). To discern how different cells behave based on EPHA2 and ROBO1 expression (see TMA stratification in Figure 3C), we examined another LSCC cell line
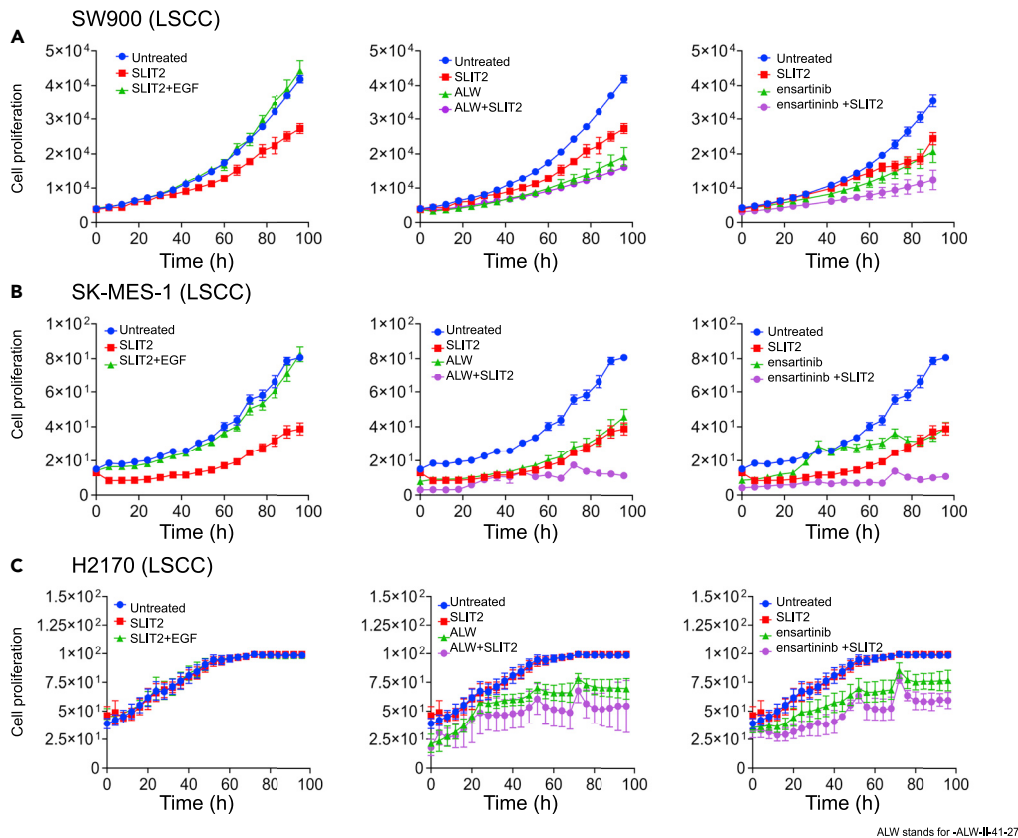
Figure 6. SLIT2/ROBO1 Interaction Negatively Regulates Cellular Proliferation in LSCC

(A) SW900 LSCC cell proliferation plot after treatment with SLIT2 (2 μg/mL), SLIT2 (2 μg/mL) + EGF (0.5 μg/mL), panel 1: ALW-II-41-27 (2 μM) and SLIT2 (2 μg/mL) + ALW-II-41-27 (2 μM), and panel 2: ensartinib (3.461 μM), SLIT2 + ensartinib panel 3.

SW900 LSCC cell proliferation plot after treatment with SLIT2 (2μg/ml), SLIT2 (2μg/ml) + EGF (0.5μg/ml), panel 1: ALW-II-41-27 (2μM) and SLIT2 (2μg/ml) + ALW-II-41-27 (2μM), and panel 2: ensartinib (3.461μM), SLIT2 + ensartinib panel 3. (B, C) SK-MES-1 and H2170 treated as in (A) with SLIT2 (2μg/ml), SLIT2 (2μg/ml) + EGF (0.5μg/ml), panel 1: ALW-II-41-27 (2μM) and SLIT2 (2μg/ml) + ALW-II-41-27 (2μM), and panel 2: ensartinib (3.461μM), SLIT2 + ensartinib panel 3. Data are represented as mean ± SD from six to eight biological replicates. One-way (ANOVA) was performed to calculate p values. Related to Figures S4 and S5.

H2170, with ROBO1^{high} and EPHA2^{low} expression. We did not see inhibition with SLIT2 but observed 30% and 22% inhibition with EPHA2 inhibitors ALW-II-47-21 and ensartinib, respectively (Figures 6C and Table 2).

A similar inhibition of proliferation was observed in HNSCC (SCC1) cells with EPHA2^{high} and ROBO1^{low} expression. Addition of SLIT2 resulted in 23% inhibition of cell proliferation that was rescued by the addition of EGF ligand (Figure 7A, panel 1). However, treating SCC1 cells with ALW-II-41-27 alone or in combination with SLIT2 showed ~20% proliferation inhibition. In the case of ensartinib treatment, either single or combination treatment resulted in ~35% inhibition indicating that the combination treatment did not have a synergistic effect (Figure 7A, panel 3, Tables 2 and 4). We also tested another HNSCC cell line SCC6 that has EPHA2^{high} and ROBO1^{low} expression. This cell line also responded to SLIT2 and ALW-II-41-27 treatments, but the effect was not synergistic (Figures 7B and Table 2). When we tested ensartinib on this cell line we did see a slight increase in inhibition with combination treatment in comparison to what we saw withSCC1 cell line. For assaying EPHA2^{low} and ROBO1^{high} expressing HNSCC cells, we tested SCC90. Again, like in LSCC, SLIT2 treatment had no discernable effect but ensartinib treatment showed 31% inhibition (Figure 7C and Table 2). SCC104, an EPHA2^{high} and ROBO1^{high} cell line, showed 46% inhibition of cell proliferation when treated with SLIT2 that was rescued by the addition of EGF ligand (Figure S6F).

LSCC	SW900 Untreated	SW900 SLIT2	SW900 SLIT2+EGF	SW900 ALW	SW900 SLIT2+ALW	SW900 Ensartinib	SW900 SLIT2+Ensartinib
% Inhibition of cellular proliferation	Control	34.56	No Inhibition	54.08	61.53	41.54	65.00
One-way (ANOVA) p values		p < 0.002 (**)	ns p < 0.1478	p < 0.0008 (***)	p < 0.0015 (**)	p < 0.0041 (**)	p < 0.0015 (**)
	SK-MES-1 Untreated	SK-MES-1 SLIT2	SK-MES-1 SLIT2+EGF	SK-MES-1 ALW	SK-MES-1 SLIT2+ALW	SK-MES-1 ensartinib	SK-MES-1 SLIT2+ensartinib
% Inhibition of cellular proliferation	Control	51.89	No Inhibition	53.13	85.52	51.63	86.12
One-way (ANOVA) p values		p < 0.0042 (**)	ns p < 0.8676	p < 0.0005 (***)	p < 0.0001 (***)	p < 0.0078 (**)	p < 0.0001 (***)
	H2170 Untreated	H2170 SLIT2	H2170 SLIT2+EGF	H2170 ALW	H2170 SLIT2+ALW	H2170 ensartinib	H2170 SLIT2+ensartinib
% Inhibition of cellular proliferation	Control	No Inhibition	No Inhibition	29.67	35.05	22.33	29.94
One-way (ANOVA) p values		ns p < 0.9997	ns p < 0.9844	p < 0.0001 (***)	p < 0.0001 (***)	p < 0.0004 (***)	p < 0.0001 (***)
LSCC	SCC1 Untreated	SCC1 SLIT2	SCC1 SLIT2+EGF	SCC1 ALW	SCC1 SLIT2+ALW	SCC1 ensartinib	SCC1 SLIT2+ensartinib
% Inhibition of cellular proliferation	Control	23.34	No Inhibition	20.66	21.63	25.59	24.75
One-way (ANOVA) p values		p < 0.0113 (*)	ns p < 0.4382	ns p < 0.1333	p < 0.0044 (**)	p < 0.0001 (***)	p < 0.0001 (***)
	SCC6 Untreated	SCC6 SLIT2	SCC6 SLIT2+EGF	SCC6 ALW	SCC6 SLIT2+ALW	SCC6 ensartinib	SCC6 SLIT2+ensartinib
% Inhibition of cellular proliferation	Control	34.87	No Inhibition	46.08	44.12	42.45	29.49
One-way (ANOVA) p values		p < 0.0001 (***)	ns p < 0.2233	ns p < 0.2713	p < 0.0052 (**)	ns p < 0.0652	p < 0.0001 (***)
	SCC90 Untreated	SCC90 SLIT2	SCC90 SLIT2+EGF	SCC90 ALW	SCC90 SLIT2+ALW	SCC90 ensartinib	SCC90 SLIT2+ensartinib
% Inhibition of cellular proliferation	Control	No Inhibition	No Inhibition	No Inhibition	No Inhibition	31.76	37.06
One-way (ANOVA) p values		ns p < 0.7553	p < 0.0065 (**)	ns p < 0.5618	ns p < 0.995	p < 0.0001 (***)	p < 0.0001 (***)

Table 2. Percentage Inhibition of LSCC and HNSCC Cell Lines on Treatment with SLIT2, ALW-II-41-27, and Ensartinib along with p Values

To discern the synergistic, additive, or antagonistic effects of combinations of SLIT2 and the EPHA2 inhibitors we performed a dose-response matrix experiment and calculated the combination index (CI) values by treating SW900 (LSCC) and SCC1 (HNSCC) cell lines with SLIT/ALW-II-41-27 and SLIT2/ensartinib treatments as described in the Transparent Methods in the Supplemental Information file. Consistent with the proliferation curves, we found that both EPHA2 inhibitors when combined with SLIT2 in LSCC showed a combination index of lower than 1 indicative of synergy (Figures S6A and S6B). In the case of HNSCC cells, for both combinations the CI values were >1 indicating antagonism (Figures S6C and S6D). These results showed that SLIT2 can inhibit proliferation in cells that are EPHA2^{high}/ROBO1^{low}, but not in EPHA2^{low}/ROBO1^{high} suggesting that SLIT2 can signal via EPHA2/ROBO1 heterodimer or an EPHA2 homodimer.

SW900 Untreated	SW900 SLIT2	SW900 SLIT2+EGF	SW900 ALW	SW900 SLIT2+ALW	SW900 Ensartinib	SW900 SLIT2+Ensartinib
	14.90	10.18	6.70	7.19	7.99	6.92
	ns p < 0.9537	ns p < 0.613	ns p < 0.6454	ns p < 0.8115	ns p < 0.3755	ns p < 0.0597
SK-MES-1 untreated	SK-MES-1 SLIT2	SK-MES-1 SLIT2+EGF	SK-MES-1 ALW	SK-MES-1 SLIT2+ALW	SK-MES-1 ensartinib	SK-MES-1 SLIT2+ensartinib
	17.98	16.28	7.41	7.29	8.43	7.25
	ns p < 0.9554	ns p < 0.4162	ns p < 0.8802	ns p < 0.5383	ns p < 0.9974	ns p < 0.9473
H2170 untreated	H2170 SLIT2	H2170 SLIT2+EGF	H2170 ALW	H2170 SLIT2+ALW	H2170 ensartinib	H2170 SLIT2+ensartinib
	11.25	16.36	1.95	1.67	12.30	11.92
	ns p < 0.4685	p < 0.0408 (*)	p < 0.0475 (*)	ns p < 0.1052	ns p < 0.3357	ns p < 0.6809
SCC1 untreated	SCC1 SLIT2	SCC1 SLIT2+EGF	SCC1 ALW	SCC1 SLIT2+ALW	SCC1 ensartinib	SCC1 SLIT2+ensartinib
	1.14	1.35	1.49	2.47	1.74	3.07
	ns p < 0.9496	ns p < 0.931	ns p < 0.9577	ns p < 0.9974	p < 0.0401 (*)	p < 0.2386
SCC6 untreated	SCC6 SLIT2	SCC6 SLIT2+EGF	SCC6 ALW	SCC6 SLIT2+ALW	SCC6 ensartinib	SCC6 SLIT2+ensartinib
	9.79	5.58	2.32	1.41	1.95	3.50
	ns p < 0.1027	ns p < 0.2364	ns p < 0.7513	ns p < 0.7506	ns p < 0.9083	ns p < 0.8686
SCC90 untreated	SCC90 SLIT2	SCC90 SLIT2+EGF	SCC90 ALW	SCC90 SLIT2+ALW	SCC90 ensartinib	SCC90 SLIT2+ensartinib
	7.01	12.72	3.54	7.62	9.78	7.27
	ns p < 0.9078	ns p < 0.3096	ns p < 0.9158	p < 0.0019 (**)	ns p < 0.4561	ns p < 0.99999

Table 3. Caspase Activity Compared with 0 h Time Point for LSCC and HNSCC Cell Lines on Treatment with SLIT2, ALW-II-41-27, and Ensartinib along with p values

It is also possible that low levels of the residual EPHA2-ROBO1 heterodimers that exist in EPHA2^{high}/ROBO1^{low} cells may form the critical threshold necessary for eliciting signaling to inhibit proliferation in ROBO1^{low} cells. As shown in the PLA experiment (Figure 5), SLIT2 can bind to EPHA2 and liganded EPHA2 may form functional homodimers to elicit signaling to inhibit cell proliferation. EPHA2 can dimerize even in the absence of ephrinA1 and stabilization of this dimer decreases the tumorigenic pS897 phosphorylation. Furthermore, a small peptide YSA, which can bind to EPHA2 and function as an agonist of the receptor, has also been reported (Singh et al., 2015, 2018; Deo et al., 2016). Another possibility is that EPHA2 may bind to another ROBO receptor or yet another receptor and inhibit proliferation. Concordant with this speculation, while this manuscript was being reviewed Volz et al. (2020) published their study where in NSCLC EPHA2 forms heterodimers with VEGF and inhibits metastasis. However, in the cell lines with EPHA2^{low} and ROBO1^{high} SLIT2 did not inhibit cell proliferation. It is a possibility that in the EPHA2^{low} cells such as H2170, a functional heterodimer may not form or, alternatively, it may not have the critical levels required for SLIT2 signaling. As discussed for the ROBO1^{low} cells, if SLIT2 is signaling via EPHA2 homodimers, these cells may not have the required levels of EPHA2 to form functional homodimers for SLIT2 signaling. EPHA2 inhibitors ALW-II-41-27 and ensartinib, on the other hand, inhibited cell proliferation by 29% and 22%, respectively, in H2170, suggesting that a small amount of EPHA2 and other RTKs that these inhibitors target could be driving cancer cell growth in these cells.

The differences in the combined effect of the treatments could be attributed to the differences in the additional pathways that are driving tumorigenesis in these cell lines or due to off target effects of one or both

Inhibitor or Ligand		Concentration		Cell Line
SLIT2		2 μg/mL		LSCC; HNSCC
EphrinA1		2 μg/mL		LSCC; HNSCC
EGF		0.5 μg/mL		LSCC; HNSCC
ALW-II-41-27		2 μM		LSCC; HNSCC
Ensartinib		3.461 μM		LSCC
Ensartinib		1.794 μM		HNSCC
LSCC	**Combination Treatments Used**	**HNSCC**	**Combination Treatments Used**	
SW900	SLIT2; SLIT2+EGF; ALW; SLIT2+ALW; ensartinib; SLIT2+ensartinib	SCC1	SLIT2; SLIT2+EGF; ALW; SLIT2+ALW; ensartinib; SLIT2+ensartinib	
SK-MES-1	SLIT2; SLIT2+EGF; ALW; SLIT2+ALW; ensartinib; SLIT2+ensartinib	SCC6	SLIT2; SLIT2+EGF; ALW; SLIT2+ALW; ensartinib; SLIT2+ensartinib	
H2170	SLIT2; SLIT2+EGF; ALW; SLIT2+ALW; ensartinib; SLIT2+ensartinib	SCC90	SLIT2; SLIT2+EGF; ALW; SLIT2+ALW; ensartinib; SLIT2+ensartinib	

Table 4. Ligand and EPHA2 Inhibitors Treatment

the drugs in the combination. Alternatively, it could be due to activation of an oncogenic kinase by disruption of a feedback loop by one of the molecules that can have an antagonistic effect on the other pathway. SLIT2 may inhibit cell proliferation by inhibiting AKT that phosphorylates S897-EPHA2, and hence, it is likely that ensartinib and ALW-II-27-41 in HNSCC can activate another kinase such as Src or PKA or inhibit a phosphatase that can increase phosphorylation of S897-EPHA2 antagonizing the effect of SLIT2. This could explain why the combination of the EPHA2 inhibitors and SLIT2 is synergistic in LSCC and antagonistic in the HNSCC. Taken together these results suggest that EPHA2 has an oncogenic role in the LSCC in the absence of its natural ligands ephrinA1 and ROBO1 has a tumor suppressor role in the presence of SLIT2 in both HNSCC and LSCC. Loss of SLIT2 leads to tumorigenesis in these cancers. In the presence of exogenously added SLIT2, EPHA2 and ROBO1 can form a complex and inhibit cell proliferation suggesting that there is cross-functional signaling between the two pathways to exert a tumor suppressor function.

Clinical Significance of ROBO1 and EPHA2 Expression and Mutations

To investigate the potential roles of EPHA2 and ROBO1 in LSCC and HNSCC, we performed overall survival analysis using GEPIA (Gene expression profiling interactive analysis) based on data from The Cancer Genome Atlas (TCGA). Percent survival of EPHA2^{low} versus EPHA2^{high} normalized to ROBO1 in LSCC showed that patients with EPHA2^{low} had better survival (60 EPHA2^{low} versus 50 EPHA2^{high} months), whereas the patients with ROBO1^{high} lived longer (65 ROBO1^{high} versus 50 ROBO1^{low} months). The log rank p value (0.082) and hazard ratio (1.3) were calculated for survival plots with EPHA2^{high} and EPHA2^{low} expressing patients normalized to ROBO1 expression. Additionally log rank p value (0.082) and hazard ratio (0.79) was calculated for ROBO1^{high} and ROBO1^{low} expressing patients normalized to EPHA2 expression (Figures S2A and S2C). In HNSCC, the survival pattern was the same, that is, EPHA2^{low} and ROBO1^{high} had better survival (75 months) in comparison with EPHA2^{high} and ROBO1^{low} (65 months). For HNSCC, the log rank p value (0.062) and hazard ratio (1.3) were calculated for survival plots with EPHA2^{high} and EPHA2^{low} expressing patients normalized to ROBO1 expression. Additionally log rank p value (0.062) and hazard ratio (0.78) was calculated for ROBO1^{high} and ROBO1^{low} expressing patients normalized to EPHA2 expression (Figures S2B and S2D). We also assayed mutations in EPHA2 and ROBO1 and their association with survival. For LSCC, EPHA2 mutations had only 19 cases with 3 deceased; therefore, the median survival could not be calculated for these. ROBO1 mutation in LSCC did not have a significant effect for survival (Figures S3A and S3C). Patients with HNSCC with alteration in EPHA2 had significantly lower survival. Again, ROBO1 alteration did not have a significant effect of survival in HNSCC (Figures S3B and S3D).
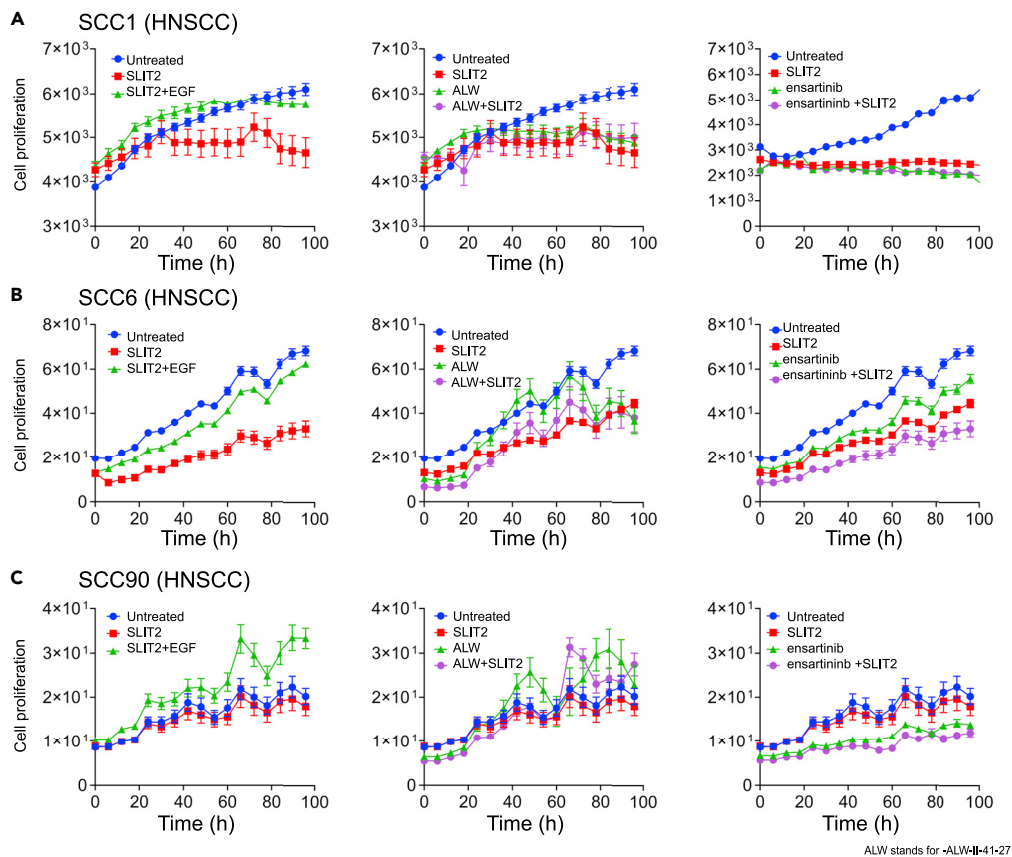
Figure 7. SLIT2/ROBO1 Interaction Negatively Regulates Cellular Proliferation in HNSCC

(A) SCC1 HNSCC cell proliferation plot after treatment with SLIT2 (2 μg/mL), SLIT2 (2 μg/mL) + EGF (0.5 μg/mL), panel 1: ALW-II-41-27 (2 μM) and SLIT2 (2 μg/mL) + ALW-II-41-27 (2 μM) panel 2, and ensartinib (1.7 μM), SLIT2 + ensartinib panel 3. SCC1 HNSCC cell proliferation plot after treatment with SLIT2 (2μg/ml), SLIT2 (2μg/ml) + EGF (0.5μg/ml), panel 1: ALW-II-41-27 (2μM) and SLIT2 (2μg/ml) + ALW-II-41-27 (2μM) panel 2, and ensartinib (1.7μM), SLIT2 + ensartinib panel 3. (B, C) SCC6 and SCC90 treated as in (A) with SLIT2 (2μg/ml), SLIT2 (2μg/ml) + EGF (0.5μg/ml), panel 1: ALW-II-41-27 (2μM) and SLIT2 (2μg/ml) + ALW-II-41-27 (2μM) panel 2, and ensartinib (1.7μM), SLIT2 + ensartinib panel 3. (The details of the individual and combination treatments are presented in Table 4. Data are represented as mean ± SD from six to eight biological replicates. p values were calculated using one-way (ANOVA). The p values are represented in Tables 2 and 3. Related to Figures S4 and S5.

DISCUSSION

RTKs play critical roles in several biological processes and have complex signaling mechanisms. Upon binding to their ligands, they often oligomerize and cross-phosphorylate each other, especially on tyrosine residues at the critical juxtamembrane domain and at the activation loop (Singh et al., 2015, 2018; Deo et al., 2016) to transduce various cellular signals. In the case of the EPH receptors, many of which are upregulated in numerous cancers, ligand activation leads to inhibition of tumor growth, migration, and invasiveness (Singh et al., 2018). In our study when SCC cells were treated with ephrinA1, the natural ligand of EPHA2 (non-tumorigenic signaling), *in vitro*, we did not see an inhibition in cellular proliferation of LSCC and HNSCC cells underscoring the need to study the presence of other degenerate, unexplored pathways regulating EPHA2 signaling (Figure S6E). Cancers overexpressing EPHA2 are accompanied by a concomitant loss of its ligands, implying that EPHA2 may act as an oncogene in the absence of its ligand. Consistent with these observations, several studies have demonstrated that EPHA2 promotes cell migration and tumor malignancy in a ligand-independent manner. This signaling is characterized by high levels of S897 phosphorylation and low levels of Y772 and Y588 phosphorylation of EPHA2 (Miao et al., 2009; Beauchamp and Debinski, 2012; Brantley-Sieders, 2012; Zhou and Sakurai, 2017). In addition to ligand-independent activation, RTK heterodimerization and examples of alternative ligands binding to atypical
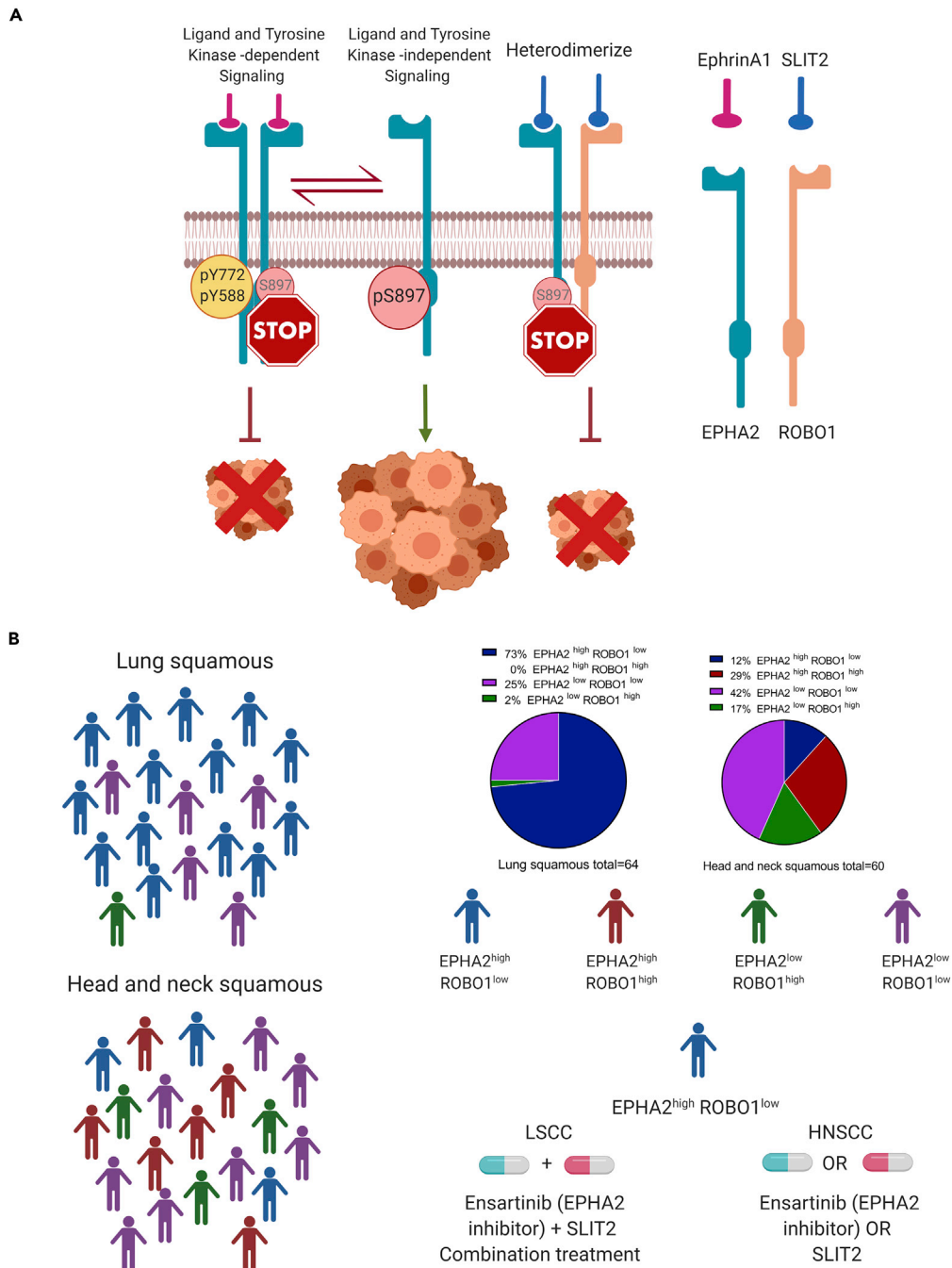
Figure 8. Mechanistic Model for SLIT2 and EPHA2-ROBO1 Signalling and Therapeutic Strategy for Patient Treatment.

(A) EPHA2, ROBO1, and SLIT form a complex. EPHA2-ROBO1 signaling model. Model of EPHA2-ROBO1 heterodimerization being stabilized in presence of SLIT2 and in turn promoting non-tumorigenic signaling highlighting therapeutic promise.

(B) Patient stratification. Treatment strategy for patients with high EPHA2 and low ROBO1 in LSCC and HNSCC.

receptors are well documented and is recognized as a means to amplify signal or induce functional diversity (Maruyama, 2014; Lemmon and Schlessinger, 2010). For example, erythropoietin, which is known to stimulate tumor growth by binding to EPHB4 despite EPHB4 not being its natural receptor (Pradeep et al., 2015).

A physical interaction between the tyrosine kinase domain-1 of VAB-1/EPHR and the CC1 region of SAX-3/ROBO has been observed in *C. elegans* (Ghenea et al., 2005). However, to the best of our knowledge, a functional heterodimer between EPHA2 and ROBO1 that can respond to SLIT2 signaling and attenuate cell proliferation in the human has not been reported thus far. We also believe that binding of SLIT2 to EPHA2, observed in the present study, has not been reported previously. Studies by Dunaway et al. (2011) have shown that cooperation between SLIT2 and ephrinA1 regulates a balance between the pro- and antiangiogenic functions of SLIT2 in mouse endothelial cells. However, no direct binding of SLIT2 to the EPHA2 receptor was shown.

To summarize our findings, we propose a model (Figure 8A) wherein ROBO1 along with SLIT2 exerts its tumor-suppressive function by heterodimerizing with EPHA2 and blocking EGF-induced phosphorylation of EPHA2 at S897 possibly by inhibiting AKT activity. In the LSCC cell line SW900 and HNSCC cell line SCC1 that expresses low levels of ROBO1, addition of SLIT2 inhibited cell proliferation (Figures 6A and 7A), suggesting that, in addition to binding to the EPHA2 and ROBO1 heterodimer (Figures 5C and 5D), SLIT2 may also bind to EPHA2 homodimers to exert its tumor suppressor effects. Alternatively, EPHA2 may heterodimerize with another ROBO receptor in ROBO1^{low} cells to inhibit cell proliferation. EPHA2 over-expression in SCCs is significantly correlated with tumor site, T classification, clinical stage, recurrence, and lymph node metastasis (Liu et al., 2012). These data highlight the translational potential of SLIT2 as a therapeutic in combination with or without EPHA2 inhibitors to treat patients with LSCC and HNSCC who currently have limited options especially those who have acquired resistance to EGFR inhibitors or have progressed on platinum-based therapy. Thus, these patients could be stratified based on the expression patterns of EPHA2 and ROBO1 proteins in the diseased tissue (Figure 8B). The vast majority of patients with LSCC (~73%) with EPHA2^{high} and ROBO1^{low} expression can be treated with a combination of SLIT2 and ensartinib, whereas those patients with EPHA2^{high} and ROBO1^{low} expression (~12%) and EPHA2^{high} and ROBO1^{high} (~29%) in HNSCC can be treated with either SLIT2 or ensartinib. Since EPHA2 and ROBO1 serve as biomarkers for discerning patients for appropriate therapy as well as therapeutic targets, they represent potential theranostics for the two diseases.

Limitations of the Study

Despite demonstrating multiple lines of evidence that EPHA2 and ROBO1 reside in the same complex and can physically interact to elicit signaling events by binding to SLIT2, more conclusive evidence using biophysical techniques such as multidimensional NMR and or X-ray crystallography is lacking. Second, the patient stratification presented here is based on EPHA2 and ROBO1 expression in TMAs. Determining the efficacy of the treatments individually and in combination in patient-derived LSCC and HNSCC cells will further validate these stratification strategies.

Resource Availability

Lead Contact

Further information and requests for resources and reagents should be directed to and will be fulfilled by the Lead Contact, Dr. Ravi Salgia (rsalgia@coh.org).

Materials Availability

This study did not generate new unique reagents.

Data and Code Availability

This study did not generate/analyze datasets/code.

METHODS

All methods can be found in the accompanying Transparent Methods supplemental file.

SUPPLEMENTAL INFORMATION

Supplemental Information can be found online at https://doi.org/10.1016/j.isci.2020.101692.

CellPress
OPEN ACCESS

ACKNOWLEDGMENTS

AUTHOR CONTRIBUTIONS

S.S.: conceptualized, performed experiments, analyzed data, wrote and reviewed the paper; K.M.P.: conceptualized, performed experiments, analyzed data, wrote and reviewed the paper; M.I.: conceptualized, performed experiments, analyzed data, wrote and reviewed the paper; M.N.: analyzed data, wrote and reviewed the paper; J.L.: analyzed data; A.N.: performed experiments, reviewed the paper; J.W.: performed experiments; I.M.: provided patient samples; R.P.: performed pathological scoring of the TMAs; A.M.: performed experiments and reviewed the paper; N.M: performed experiments, analyzed data; A.B.: conceptualized, wrote and reviewed the paper; P.K.: conceptualized, reviewed and wrote the paper; D.L.W.: conceptualized the idea, reviewed the paper; R,S.: conceptualized the idea, reviewed the paper.

DECLARATION OF INTERESTS

The authors declare no competing interests.

REFERENCES

Adjei, A.A. (2019). Lung cancer worldwide. J. Thorac. Oncol. *14*, 956.

Amato, K.R., Wang, S., Tan, L., Hastings, A.K., Song, W., Lovly, C.M., Meador, C.B., Ye, F., Lu, P., Balko, J.M., et al. (2016). EPHA2 blockade overcomes acquired resistance to EGFR kinase inhibitors in lung cancer. Cancer Res. *76*, 305–318.

Amato, K.R., Wang, S., Hastings, A.K., Youngblood, V.M., Santapuram, P.R., Chen, H., Cates, J.M., Colvin, D.C., Ye, F., Brantley-Sieders, D.M., et al. (2014). Genetic and pharmacologic inhibition of EPHA2 promotes apoptosis in NSCLC. J. Clin. Invest. *124*, 2037–2049.

Ballard, M.S., and Hinck, L. (2012). A roundabout way to cancer. Adv. Cancer Res. *114*, 187–235.

Beauchamp, A., and Debinski, W. (2012). EPHs and ephrins in cancer: ephrin-A1 signalling. Semin. Cell Dev. Biol. *23*, 109–115.

Bedell, V.M., Yeo, S.Y., Park, K.W., Chung, J., Seth, P., Shivalingappa, V., Zhao, J., Obara, T., Sukhatme, V.P., Drummond, I.A., et al. (2005). Roundabout4 is essential for angiogenesis in vivo. Proc. Natl. Acad. Sci. U S A. *102*, 6373–6378.

Bernadskaya, Y.Y., Wallace, A., Nguyen, J., Mohler, W.A., and Soto, M.C. (2012). UNC-40/DCC, SAX-3/Robo, and VAB-1/Eph polarize F-actin during embryonic morphogenesis by regulating the WAVE/SCAR actin nucleation complex. Plos Genet. *8*, 1–17.

Blockus, H., and Chédotal, A. (2016). SLIT-ROBO signaling. Development *143*, 3037–3044.

Boyd, A.W., Bartlett, P.F., and Lackmann, M. (2014). Therapeutic targeting of EPH receptors and their ligands. Nat. Rev. Drug Discov. *13*, 39–62.

Brand, T.M., Iida, M., Li, C., and Wheeler, D.L. (2011). The nuclear epidermal growth factor receptor signaling network and its role in cancer. Discov. Med. *12*, 419–432.

Brand, T.M., Iida, M., Luthar, N., Starr, M.M., Huppert, E.J., and Wheeler, D.L. (2013). Nuclear EGFR as a molecular target in cancer. Radiother. Oncol. *108*, 370–377.

Brand, T.M., Iida, M., Stein, A.P., Corrigan, K.L., Braverman, C.M., Coan, J.P., Pearson, H.E., Bahrar, H., Fowler, T.L., Bednarz, B.P., et al. (2015). AXL is a logical molecular target in head and neck squamous cell carcinoma. Clin. Cancer Res. *21*, 2601–2612.

Brantley-Sieders, D.M. (2012). Clinical relevance of EPHs and ephrins in cancer: lessons from breast, colorectal, and lung cancer profiling. Semin. Cell Dev. Biol. *23*, 102–108.

Bray, F., Ferlay, J., Soerjomataram, I., Siegel, R.L., Torre, L.A., and Jemal, A. (2018). Global cancer statistics: GLOBOCAN estimates of incidence and mortality worldwide for 36 cancers in 185 countries. CA Cancer J. Clin. *68*, 394–424.

Chang, P.H., Hwang-Verslues, W.W., Chang, Y.C., Chen, C.C., Hsiao, M., Jeng, Y.M., Chang, K.J., Lee, E.Y., Shew, J.Y., and Lee, W.H. (2012). Activation of Robo1 signaling of breast cancer cells by Slit2 from stromal fibroblast restrains tumorigenesis via blocking PI3K/Akt/β-catenin pathway. Cancer Res. *72 18*, 4652–4661.

Chen, H., Zhang, M., Tang, S., London, N.R., Li, D.Y., and Zhang, K. (2010). SLIT-ROBO signaling in ocular angiogenesis. Adv. Exp. Med. Biol. *664*, 457–463.

Chin-Sang, I.D., George, S.E., Ding, M., Moseley, S.M., Lynch, A.S., and Chisholm, A.D. (1999). The Ephrin VAB-2/EFN-1 functions in neuronal signaling to regulate epidermal morphogenesis in *C. elegans*. Cell *99*, 781–790.

Choi, Y., Syeda, F., Walker, J.R., Finerty, P.J., Jr., Cuerrier, D., Wojciechowski, A., Liu, Q., Dhe-Paganon, S., and Gray, N.S. (2009). Discovery and structural analysis of Eph receptor tyrosine kinase

inhibitors. Bioorg. Med. Chem. Lett. *19*, 4467–4470.

Dallol, A., Da Silva, N.F., Viacava, P., Minna, J.D., Bieche, I., Maher, E.R., and Latif, F. (2002). SLIT2, a human homologue of the Drosophila Slit2 gene, has tumor suppressor activity and is frequently inactivated in lung and breast cancers. Cancer Res. *62*, 5874–5880.

Darling, T.K., and Lamb, T.J. (2019). Emerging roles for Eph receptors and ephrin ligands in immunity. Front. Immunol. *10*, 1–15.

Deo, R., Singh, D.R., Pasquale, E.B., and Hristova, K. (2016). A small peptide promotes EphA2 kinase-dependent signaling by stabilizing EphA2 dimers. Biochim. Biophys. Acta *1860*, 1922–1928.

Dunaway, C.M., Hwang, Y., Lindsley, C.W., Cook, R.S., Wu, J.Y., Boothby, M., Chen, J., and Brantley-Sieders, D.M. (2011). Cooperative signaling between Slit2 and Ephrin-A1 regulates a balance between angiogenesis and angiostasis. Mol. Cell. Biol. *31*, 404–416.

Fang, W.B., Brantley-Sieders, D.M., Parker, M.A., Reith, A.D., and Chen, J. (2005). A kinase-dependent role for EPHA2 receptor in promoting tumor growth and metastasis. Oncogene *24*, 7859–7868.

Fang, W.B., Brantley-Sieders, D.M., Hwang, Y., AJ Ham, A.J., and Chen, J. (2008). Identification and functional analysis of phosphorylated tyrosine residues within EphA2 receptor tyrosine kinase. J. Biol. Chem. *283*, 16017–16026.

Faoro, L.1., Singleton, P.A., Cervantes, G.M., Lennon, F.E., Choong, N.W., Kanteti, R., Ferguson, B.D., Husain, A.N., Tretiakova, M.S., Ramnath, N., et al. (2010). EPHA2 mutation in lung squamous cell carcinoma promotes increased cell survival, cell invasion, focal adhesions, and mammalian target of rapamycin activation. J. Biol. Chem. *285*, 18575–18585.

Ferguson, B.D., Liu, R., Rolle, C.E., Tan, Y.H., Krasnoperov, V., Kanteti, R., Tretiakova, M.S., Cervantes, G.M., Hasina, R., Hseu, R.D., et al. (2013). The EPHB4 receptor tyrosine kinase promotes lung cancer growth: a potential novel therapeutic target. PLoS One *8*, 67668.

Fukazawa, T., Guo, M., Ishida, N., Yamatsuji, T., Takaoka, M., Yokota, E., Haisa, M., Miyake, N., Ikeda, T., Okui, T., et al. (2016). SOX2 suppresses CDKN1A to sustain growth of lung squamous cell carcinoma. Sci. Rep. *6*, 20113.

Gara, R.K., Kumari, S., Ganju, A., Yallapu, M.M., Jaggi, M., and Chauhan, S.C. (2015). SLIT/ROBO pathway: a promising therapeutic target for cancer. Drug Discov. Today *20*, 156–164.

Gomes, D.A., Rodrigues, M.A., Leite, M.F., Gomez, M.V., Varnai, P., Balla, T., Bennett, A.M., and Nathanson, M.H. (2008). c-Met must translocate to the nucleus to initiate calcium signals. J. Biol. Chem. *283*, 4344–4351.

Grieshammer, U., Ma, L., Plump, A.S., Wang, F., Tessier-Lavigne, M., and Martin, G.R. (2004). SLIT2-mediated ROBO2 signaling restricts kidney induction to a single site. Dev. Cell *6*, 709–717.

George, S.E., Simokat, K., Hardin, J., and Chisholm, A.D. (1998). The VAB-1 Eph receptor

tyrosine kinase functions in neural and epithelial morphogenesis in *C. elegans*. Cell *92*, 633–643.

Ghenea, S., Boudreau, J.R., Lague, N.P., and Chin-Sang, I.D. (2005). The VAB-1 EPH receptor tyrosine kinase and SAX-3/ROBO neuronal receptors function together during *C. elegans* embryonic morphogenesis. Development *132*, 3679–3690.

Herbst, R.S., Morgensztern, D., and Boshoff, C. (2018). The biology and management of non-small cell lung cancer. Nature *553*, 446–454.

Hohenester, E. (2008). Structural insight into SLIT-ROBO signalling. Biochem. Soc. Trans. *36*, 251–256.

Horn, L., Infante, J.R., Reckamp, K.L., Blumenschein, G.R., Leal, T.A., Waqar, S.M., Gitlitz, B.J., Sanborn, R.E., Whisenant, J.G., Du, L., et al. (2018). Ensartinib (X-396) in ALK-positive non-small cell lung cancer: results from a first-in-human phase I/II, multicenter study. Clin. Cancer Res. *24*, 2771–2779.

Huang, Z., Wen, P., Kong, R., Cheng, H., Zhang, B., Quan, C., Bian, Z., Chen, M., Zhang, Z., Chen, X., et al. (2015). USP33 mediates SLIT-ROBO signaling in inhibiting colorectal cancer cell migration. Int. J. Cancer *136*, 1792–1802.

Johnson, C., Segovia, B., and Kandpal, R.P. (2016). EPHA7 and EPHA10 physically interact and differentially Co-localize in normal breast and breast carcinoma cell lines, and the Co-localization pattern is altered in EPHB6-expressing MDA-MB-231 cells. Cancer Genomics Proteomics *13*, 359–368.

Kidd, T., Bland, K.S., and Goodman, C.S. (1999). SLIT is the midline repellent for the ROBO receptor in Drosophila. Cell *19*, 785–794.

Koch, H., Busto, M.E., Kramer, K., Médard, G., and Kuster, B. (2015). Chemical proteomics uncovers EPHA2 as a mechanism of acquired resistance to small molecule EGFR kinase inhibition. J. Proteome Res. *14*, 2617–2625.

Lemmon, M., and Schlessinger, A.J. (2010). Cell signaling by receptor tyrosine kinases. Cell *141*, 1117–1134.

Lisabeth, E.M., Falivelli, G., and Pasquale, E.B. (2013). Eph receptor signaling and ephrins. Cold Spring Harb. Perspect. Biol. *5*, 1–20.

Liu, Y., Yu, C., Qiu, Y., Huang, D., Zhou, X., Zhang, X., and Tian, Y. (2012). Downregulation of EphA2 expression suppresses the growth and metastasis in squamous-cell carcinoma of the head and neck in vitro and *in vivo*. J. Cancer Res. Clin. Oncol. *138*, 195–202.

Maiti, G.P., Ghosh, A., Mondal, P., Ghosh, S., Chakraborty, J., Roy, A., Roy Chowdhury, S., and Panda, C.K. (2015). Frequent inactivation of SLIT2 and ROBO1 signaling in head and neck lesions: clinical and prognostic implications. Oral Surg. Oral Med. Oral Pathol. Oral Radiol. *119*, 202–212.

Maruyama, I.N. (2014). Mechanisms of activation of receptor tyrosine kinases: monomers or dimers. Cells *3*, 304–330.

Miao, H., Li, D.Q., Mukherjee, A., Guo, H., Petty, A., Cutter, J., Basilion, J.P., Sedor, J., Wu, J., Danielpour, D., et al. (2009). EPHA2 mediates

ligand-dependent inhibition and ligand-independent promotion of cell migration and invasion via a reciprocal regulatory loop with Akt. Cancer Cell *16*, 9–20.

Miao, B., Ji, Z., Tan, L., Taylor, J.M., Zhang, J., Choi, H.G., Frederick, D.T., Kumar, R., Wargo, J.A., Flaherty, K.T., et al. (2015). EphA2 is a mediator of vemurafenib resistance and a novel therapeutic target in melanoma. Cancer Discov. *5*, 274–287.

Mosch, B., Reissenweber, B., Neuber, C., and Pietzsch, J. (2010). Eph receptors and Ephrin ligands: important players in angiogenesis and tumor angiogenesis. J. Oncol. *2010*, 135285.

Pasquale, E.B. (2010). EPH receptors and ephrins in cancer: bidirectional signaling and beyond. Nat. Rev. Cancer *10*, 165–180.

Pradeep, S., Huang, J., Mora, E.M., Nick, A.M., Cho, M.S., Wu, S.Y., Noh, K., Pecot, C.V., Rupaimoole, R., Stein, M.A., et al. (2015). Erythropoietin stimulates tumor growth via EPHB4. Cancer Cell *28*, 610–622.

Rothberg, J.M., Hartley, D.A., Walther, Z., and Artavanis-Tsakonas, S. (1988). SLIT: an EGF-homologous locus of D. melanogaster involved in the development of the embryonic central nervous system. Cell *23*, 1047–1059.

Sabari, J.K., and Paik, P.K. (2017). Relevance of genetic alterations in squamous and small cell lung cancer. Ann. Transl. Med. *5*, 373–386.

Salgia, R., and Kulkarni, P. (2018). The genetic/ non-genetic duality of drug 'resistance' in cancer. Trends Cancer *4*, 110–118.

Seki, M., Watanabe, A., Enomoto, S., Kawamura, T., Ito, H., Kodama, T., Hamakubo, T., and Aburatani, H. (2010). Human ROBO1 is cleaved by metalloproteinases and gamma-secretase and migrates to the nucleus in cancer cells. FEBS Lett. *584*, 2909–2915.

Siegel, R.L., Miller, K.D., and Jemal, A. (2020). Cancer statistics. CA Cancer J. Clin. *70*, 7.

Singh, A., Winterbottom, E., and Daar, I.O. (2012). Eph/ephrin signaling in cell-cell and cell-substrate adhesion. Front. Biosci. (Landmark Ed.) *17*, 473–497.

Singh, D.R., Ahmed, F., King, C., Gupta, N., Salotto, M., Pasquale, E.B., and Hristova, K. (2015). EPHA2 receptor nnliganded dimers suppress EPHA2 pro-tumorigenic signaling. J. Biol. Chem. *290*, 27271–27279.

Singh, D.R., Kanvinde, P., King, C., Pasquale, E.B., and Hristova, K. (2018). The EPHA2 receptor is activated through induction of distinct, ligand-dependent oligomeric structures. Commun. Biol. *22*, 1–15.

Stammes, M.A., Prevoo, H.A., Ter Horst, M.C., Groot, S.A., Van de Valde, C.J.H., Chan, A.B., de Gues-OeL-, F., Kuppen, P.J.K., Vahrmeijer, A.L., Pasquale, E.B., and Sier, C.F.M. (2017). Evaluation of EphA2 and EphB4 as targets for image-guided colorectal cancer Surgery. Int. J. Mol. Sci. *18*, 307–316.

Strickland, P., Shin, G.C., Plump, A., Tessier-Lavigne, M., and Hinck, L. (2006). SLIT2 and netrin 1 act synergistically as adhesive cues to generate

tubular bi-layers during ductal morphogenesis. Development *133*, 823–832.

Taddei, M.L., Parri, M., Angelucci, A., Onnis, B., Bianchini, F., Giannoni, E., Raugei, G., Calorini, L., Rucci, N., Teti, A., et al. (2009). Kinase-dependent and -independent roles of EPHA2 in the regulation of prostate cancer invasion and metastasis. Am. J. Pathol. *174*, 1492–1503.

Tan, Y.C., Srivastava, S., Won, B.M., Kanteti, R., Arif, Q., Husain, A.N., Li, H., Vigneswaran, W.T., Pang, K.M., Kulkarni, P., et al. (2019). EPHA2 mutations with oncogenic characteristics in squamous cell lung cancer and malignant pleural mesothelioma. Oncogenesis *8*, 49–60.

Tey, S.K., Tse, E.Y.T., Mao, X., Ko, F.C.F., Wong, A.S.T., Lo, R.C., Ng, I.O., and Yam, J. (2017). W. P. Nuclear Met promotes hepatocellular carcinoma tumorigenesis and metastasis by upregulation of TAK1 and activation of NF-κB pathway. Cancer Lett. *411*, 150–161.

Volz, C., Breid, S., Selenz, C., Zaplatina, A., Golfmann, K., Meder, L., Dietlein, F., Borchmann, S., Chatterjee, S., Siobal, M., et al. (2020). Inhibition of tumor VEGFR2 induces serine 897

EphA2-dependent tumor cell invasion and metastasis in NSCLC. Cell Rep. *31*, 107568.

Wang, S.C., and Hung, M.C. (2009). Nuclear translocation of the epidermal growth factor receptor family membrane tyrosine kinase receptors. Clin. Cancer Res. *15*, 6484–6489.

Xian, J., Clark, K.J., Fordham, R., Pannell, R., Rabbitts, T.H., and Rabbitts, P.H. (2001). Inadequate lung development and bronchial hyperplasia in mice with a targeted deletion in the Dutt1/ROBO1 gene. Proc. Natl. Acad. Sci. U S A *18*, 15062–15066.

Xie, Y., Nurkesh, A.A., Ibragimova, N., Zhanzak, Z., Meyerbekova, A., Alexeyeva, Z., Yesbolatova, A., Satayeva, M., Mustafa, A., Manarbek, L., et al. (2019). Systematic analysis of NLMP suggests nuclear localization of RTK/MET kinases resemble cancer cell clearance. J. Exp. Clin. Cancer Res. *38*, 43–54.

Xie, Y., Lu, W., Liu, S., Yang, Q., Carver, B.S., Li, E., Wang, Y., Fazli, L., Gleave, M., and Chen, Z. (2014). Crosstalk between nuclear MET and SOX9/β-catenin correlates with castration-resistant prostate cancer. Mol. Endocrinol. *28*, 1629–1639.

Zappa, C., and Mousa, S.A. (2016). Non-small cell lung cancer: current treatment and future advances. Transl. Lung Cancer Res. *5*, 288–300.

Zelinski, D.P., Zantek, N.D., Stewart, J.C., Irizarry, A.R., and Kinch, M.S. (2001). EPHA2 overexpression causes tumorigenesis of mammary epithelial cells. Cancer Res. *61*, 2301–2306.

Zhou, Y., and Sakurai, H. (2017). Emerging and diverse functions of the EPHA2 noncanonical pathway in cancer progression. Biol. Pharm. Bull. *40*, 1616–1624.

Zhou, Y., Yamada, N., Tanaka, T., Hori, T., Yokoyama, S., Hayakawa, Y., Yano, S., Fukuoka, J., Koizumi, K., Saiki, I., and Sakurai, H. (2015). Crucial roles of RSK in cell motility by catalysing serine phosphorylation of EPHA2. Nat. Commun. *6*, 7679.

Zhuang, G., Brantley-Sieder, s D.M., Vaught, D., Yu, J., Xie, L., Wells, S., Jackson, D., Muraoka-Cook, R., Arteaga, C., and Chen, J. (2010). Elevation of receptor tyrosine kinase EPHA2 mediates resistance to trastuzumab therapy. Cancer Res. *70*, 299–308.

Supplemental Information

Activation of EPHA2-ROBO1 Heterodimer

by SLIT2 Attenuates Non-canonical Signaling

and Proliferation in Squamous Cell Carcinomas

Saumya Srivastava, Ka Ming Pang, Mari Iida, Michael S. Nelson, Jiayi Liu, Arin Nam, Jiale Wang, Isa Mambetsariev, Raju Pillai, Atish Mohanty, Nellie McDaniel, Amita Behal, Prakash Kulkarni, Deric L. Wheeler, and Ravi Salgia

Figure S1: VAB-1 and SAX-3 pathways are synthetic lethal in *C. elegans*: (A, and B): RNA interference experiment of VAB-1(EPHA2) and SAX-3 (ROBO1) to determine embryonic lethality in comparison to wild type worms N2. (**C**): Table indicating F1 progeny which survived in (**A and B**) out of total worms. (**D**) The synthetic lethal phenotype is also seen with SAX-3 RNAi and use of an EPHA2 inhibitor ALW-II-41-27. The p-value was calculated using one-way ANOVA. N2+ALW-II-41-27 have significant worm death (p <0.0001) in comparison to untreated N2 worms. Sax-3 RNAi+ALW-II-41-27 has more worm death than control (p <0.0001). Biological replicates indicated in table. Data are represented as mean ± SD. Related to Fig. 1 and 2.

A — *vab-1* RNAi

B — *sax3* RNAi

C

n=400	Percentage viable
N2 vab-1RNAi	99.8
ky200 vab-1RNAi	39.7
ky123 vab-1 RNAi	13.5
N2 sax-3 RNAi	100
OK1699 sax-3 RNAi	6.3
e2 sax-3 RNAi	65.5
e2027 sax-3 RNAi	36.6

D
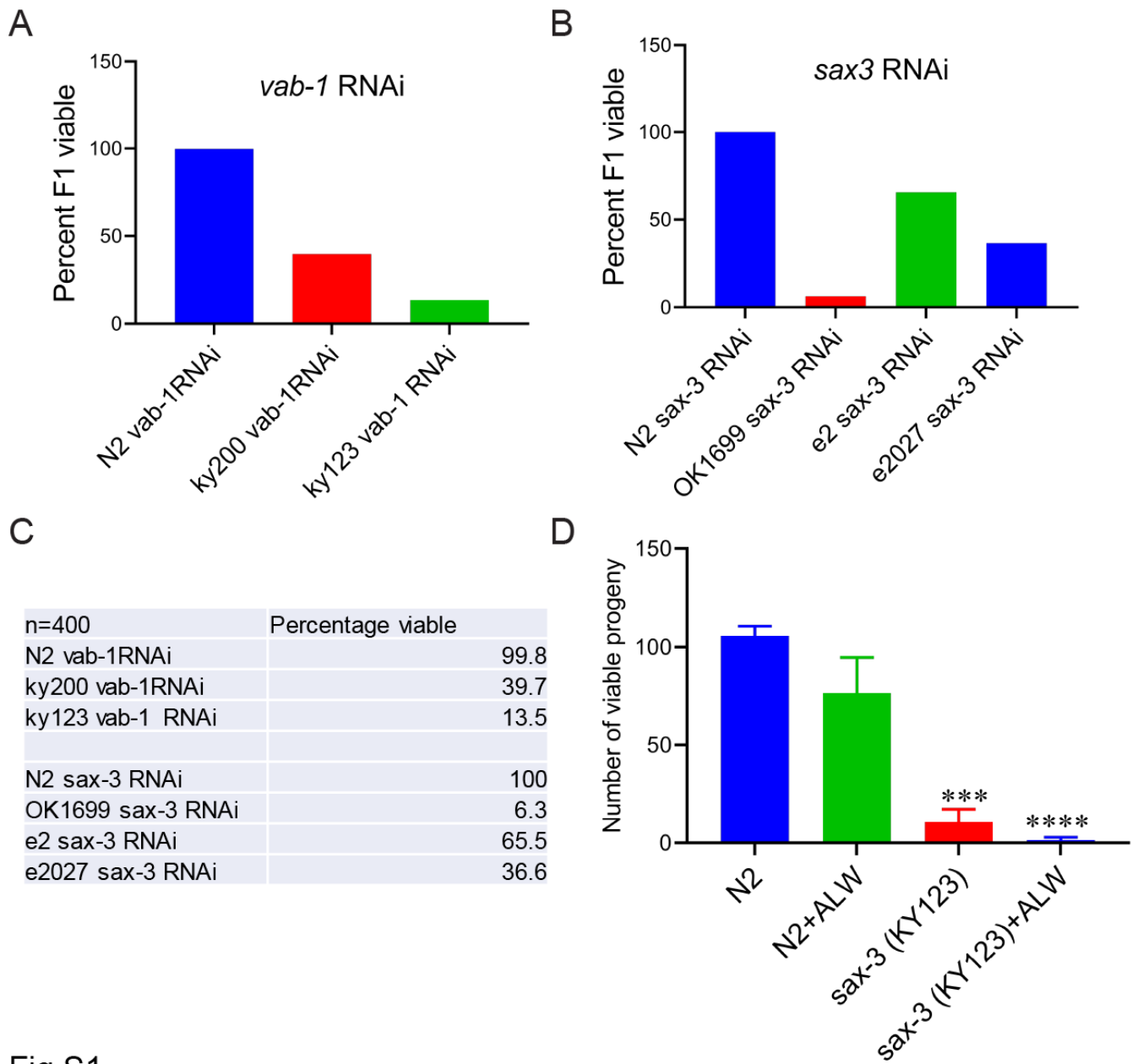
Fig S1

Fig S2: Clinical significance of ROBO1 and EPHA2 expression. (**A**) LSCC overall survival comparison of low and high EPHA2 expressing patients, normalized to median expression level of ROBO1. (**B**) HNSCC overall survival comparison of low and high EPHA2 expressing patients, normalized to median expression level of ROBO1. (**C**) LSCC overall survival comparison of low and high ROBO1 expressing patients, normalized to median expression level of EPHA2. (**D**) HNSCC overall survival comparison of low and high ROBO1 expressing patients, normalized to median expression level of EPHA2. Hazard ratio and p-value calculated indicated in the plot. Related to Fig. 3.
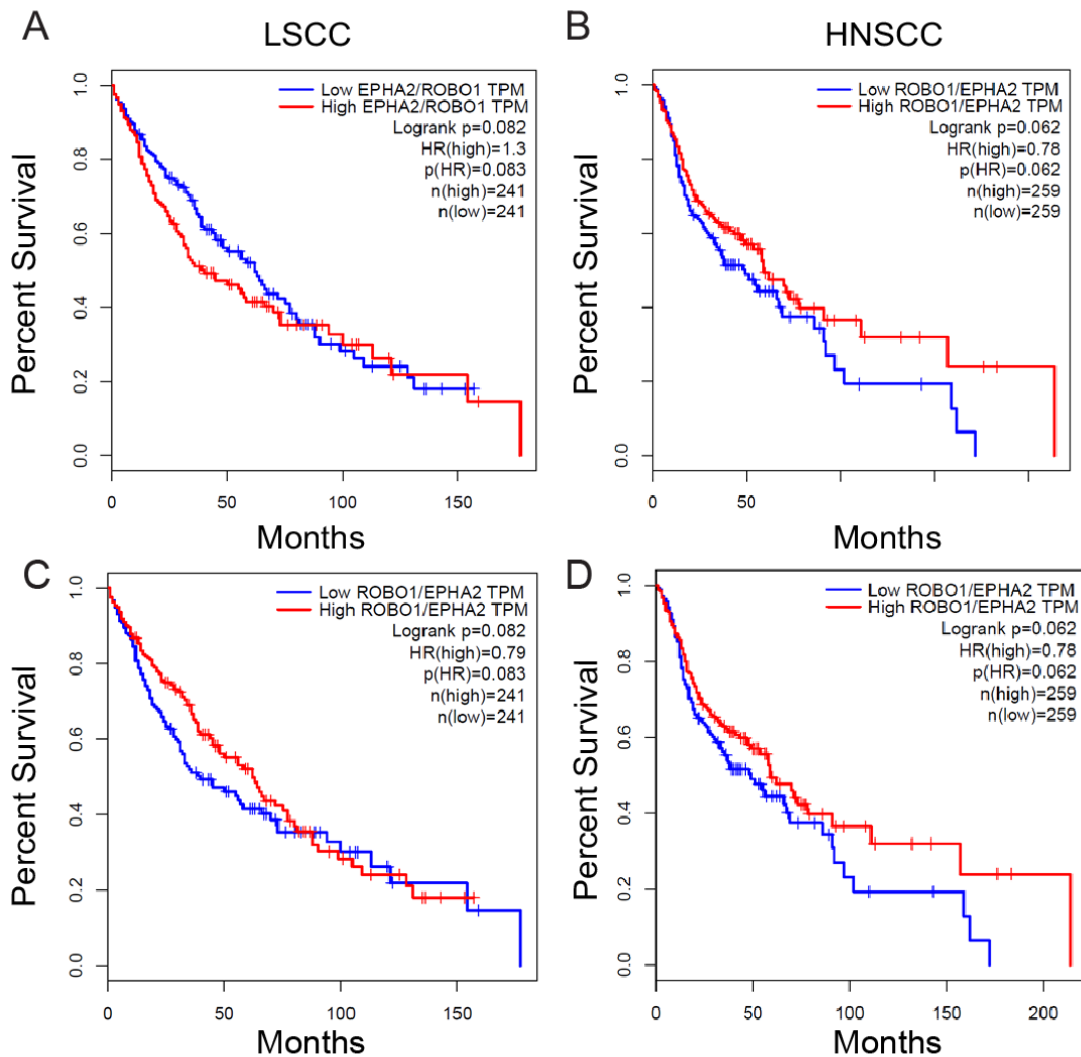

Fig S2

Fig S3: Different mutations and associated survival for EPHA2 and ROBO1 in LSCC and HNSCC. (A and C) LSCC: EPHA2 and ROBO1 distribution of different mutations and their associated survival. **(B and D)** HNSCC: EPHA2 and ROBO1 distribution of different mutations and their associated survival. Related to Fig. 3.

A — EPHA2 LSCC

Logrank Test P-Value-0.0614

Group	# of Cases, Total	# of Cases, Deceased	MMS
Altered	19	3	NA
Unaltered	960	418	54.40

- Mutations
- Amplifications
- Deep Deletions
- Multiple Alterations

B — EPHA2 HNSCC

Logrank Test P-Value-0.0526

Group	# of Cases, Total	# of Cases, Deceased	MMS
Altered	59	29	37.25
Unaltered	1148	482	56.90

C — ROBO1 LSCC

Logrank Test P-Value-0.382

Group	# of Cases, Total	# of Cases, Deceased	MMS
Altered	72	26	60.53
Unaltered	907	395	54.40

D — ROBO1 HNSCC

Logrank Test P-Value-0.968

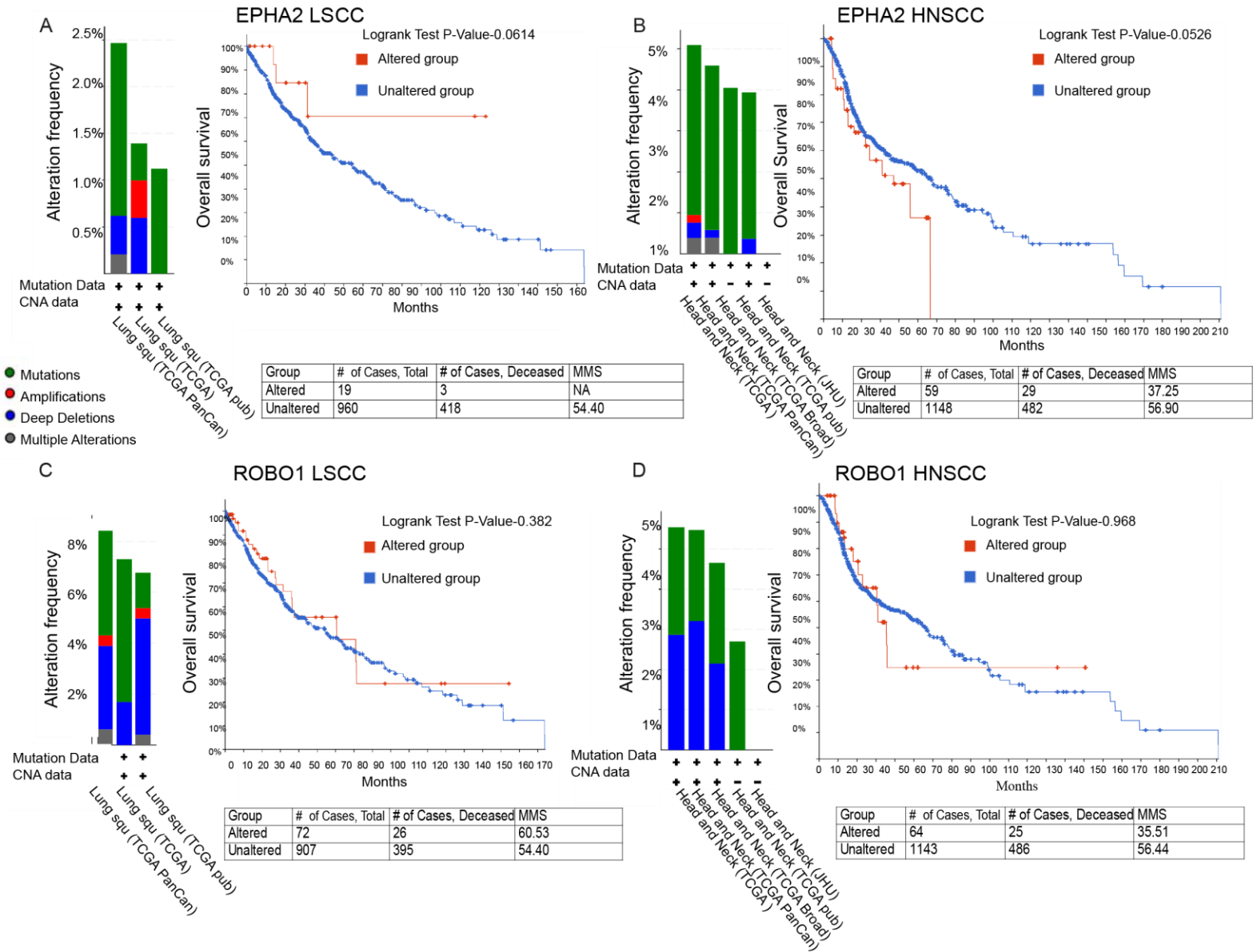| Group	# of Cases, Total	# of Cases, Deceased	MMS
Altered	64	25	35.51
Unaltered	1143	486	56.44

Fig S3

Fig S4: Caspase activity plot to all proliferation plots represented in Fig. 6. (A, B and C) SW900, SK-MES-1 and H2170, LSCC cell lines caspase activity plot after treatment with SLIT2 (2μg/ml) and SLIT2+EGF(0.5μg/ml) panel 1; SLIT2 (2μg/ml), ALW-II-41-27 (2μM) SLIT2+ALW-II-41-27 panel 2 and ensartinib 3.461μM and SLIT2+Ensartinib combination treatment panel 3. For each experiment, 6-8 biological replicates were examined. Data are represented as mean ± SD. The p-value was calculated using One-way (ANOVA). See also Table 3 for p-values. Related to Fig. 6.

Fig S4

Fig S5: Caspase activity plot to all proliferation plots represented in Fig. 7. (A, B and C) SCC1, SCC6 and SCC90, HNSCC cell lines caspase activity plot after treatment with SLIT2 (2μg/ml) and EGF(0.5μg/ml) panel 1; SLIT2 (2μg/ml), ALW-II-41-27 (2μM) and SLIT2+ALW-II-41-27 panel 2 and ensartinib 1.79 μM and SLIT2+ensartinib combination treatment panel 3. For each experiment, 6-8 biological replicates were examined. Data are represented as mean ± SD. The p-value was calculated using One-way (ANOVA). See also Table 3 for p-values. Related to Fig. 7.
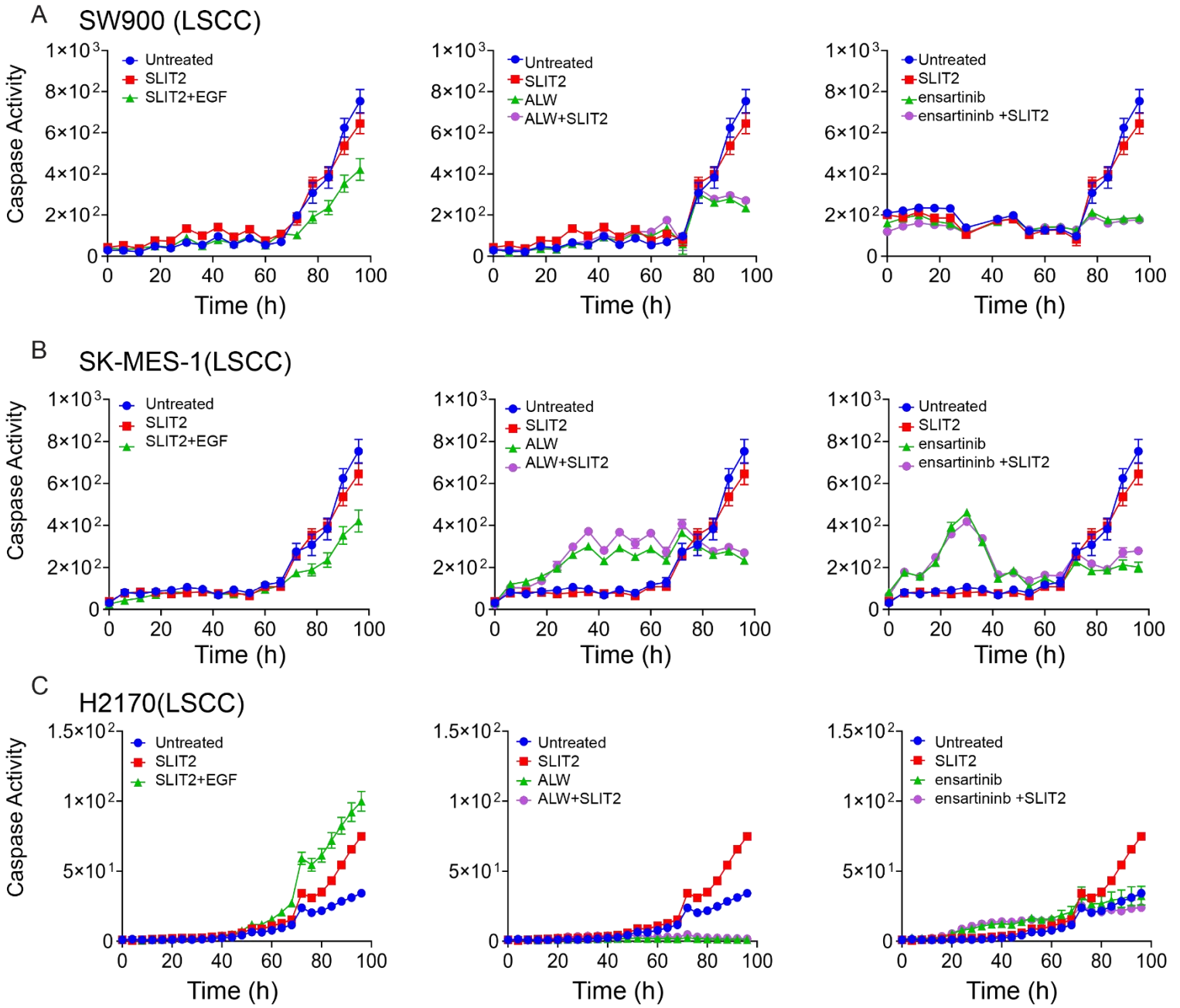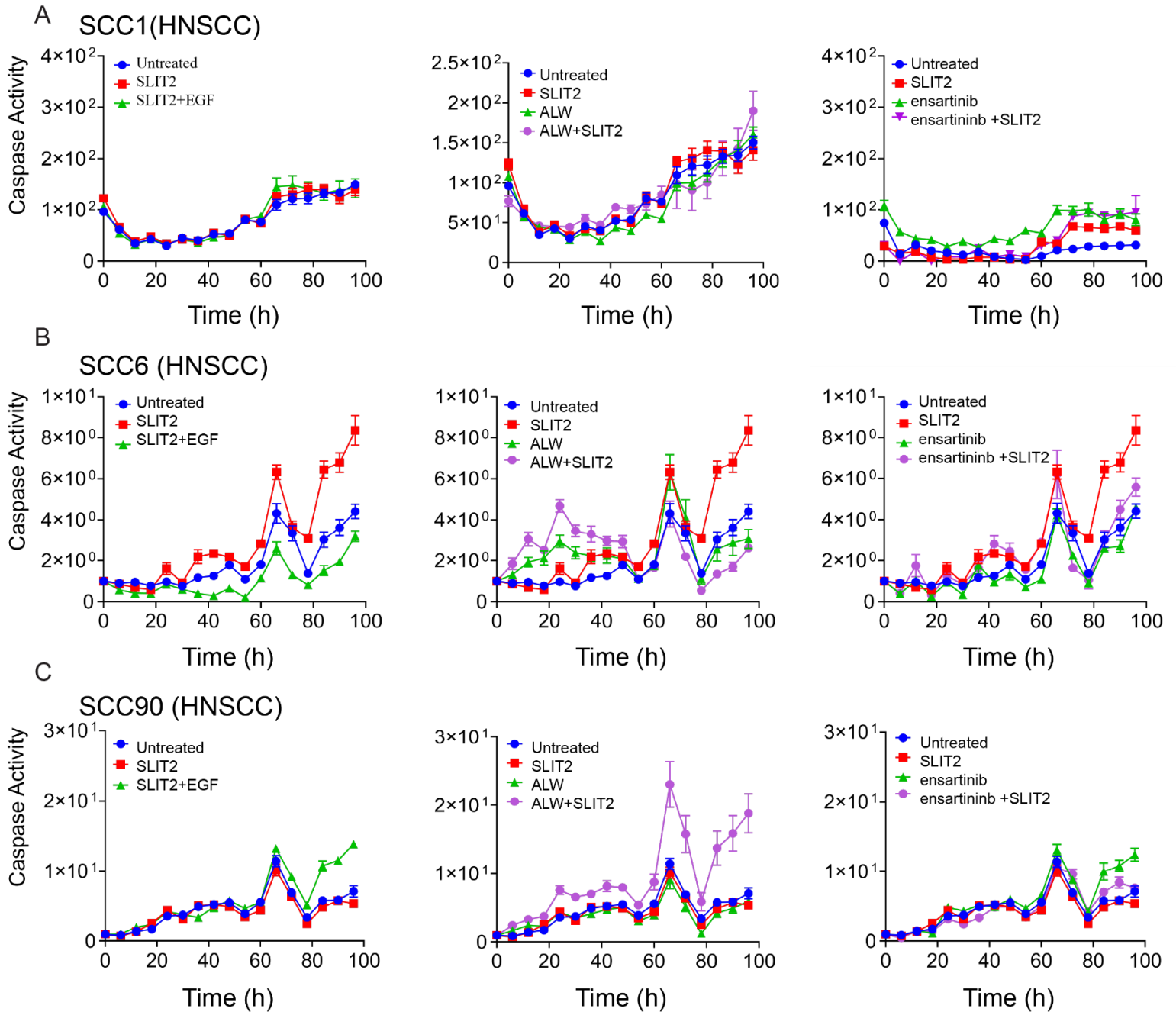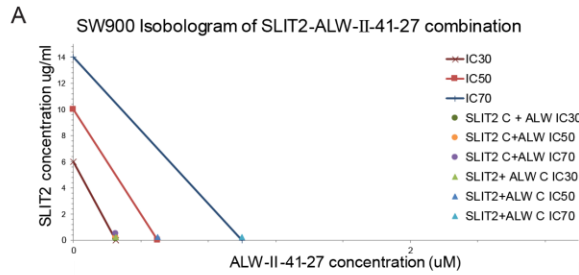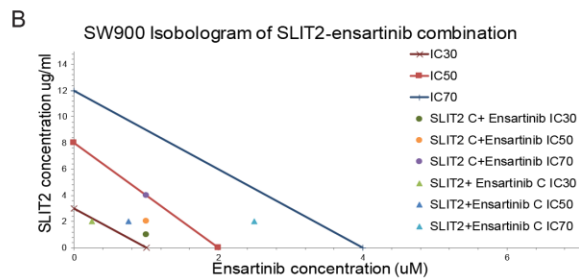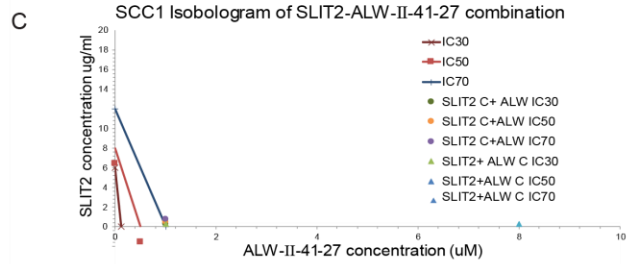
Fig S6: Combination index; EphrinA1 treatment in SW900 and SCC1; SCC104 proliferation and caspase activity plot; Fig. 4B immunofluorescence negative control. Combination index Isobolograms.: (**A, and B**). SW900 (LSCC) Isobologram and table of combination index values for SLIT2-ALW-II-41-27 treatment and SLIT2-ensartininb treatment for IC30, 50 and 70. (**C, and D**). SCC1 (HNSCC) Isobologram and table of combination index values for SLIT2-ALW-II-41-27 treatment and SLIT2-ensartininb treatment for IC30, 50 and 70. (**E**) SW900 (LSCC) and SCC1 (HNSCC) proliferation plot comparing ephrinA1 and SLIT2 treatment. Eight biological replicates were used. P-value was calculated using one-way ANOVA. Both the plots show there is no effect of ephrinA1 treatment. But the inhibition in proliferation after SLIT2 treatment is significant ($p < 0.0001$). Data are represented as mean ± SD. (**F**) SCC104 proliferation and caspase activity plot after SLIT2 ($2\mu g/ml$) and SLIT2+EGF ($0.5\mu g/ml$) treatment p-value was calculated using One-way ANOVA. Data are represented as mean ± SD. Eight biological replicates were used. (**G**) Negative controls for **Fig. 4B** showing only secondary Alexa Flour 547 (red) staining and secondary Alexa Flour 488 (green) staining. Images were taken at 40X magnification. Scale bar =$10\mu m$. Related to Fig. 6 and 7.
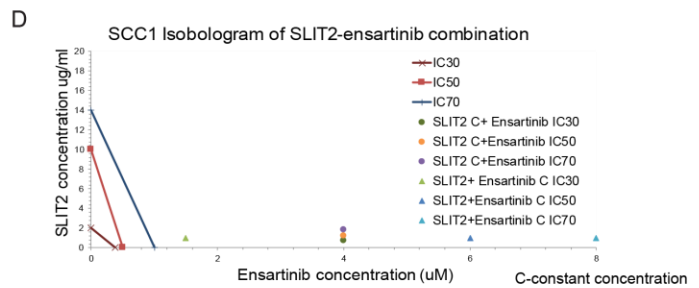
A SW900 Isobologram of SLIT2-ALW-II-41-27 combination

Legend:
- IC30
- IC50
- IC70
- SLIT2 C + ALW IC30
- SLIT2 C+ALW IC50
- SLIT2 C+ALW IC70
- SLIT2+ ALW C IC30
- SLIT2+ALW C IC50
- SLIT2+ALW C IC70

Y-axis: SLIT2 concentration ug/ml
X-axis: ALW-II-41-27 concentration (uM)

COMBINATION I (SLIT2 +ALW)	CI Values
IC	CI
30	1.02
50	0.53
70	0.29

C SCC1 Isobologram of SLIT2-ALW-II-41-27 combination

Legend:
- IC30
- IC50
- IC70
- SLIT2 C+ ALW IC30
- SLIT2 C+ALW IC50
- SLIT2 C+ALW IC70
- SLIT2+ ALW C IC30
- SLIT2+ALW C IC50
- SLIT2+ALW C IC70

Y-axis: SLIT2 concentration ug/ml
X-axis: ALW-II-41-27 concentration (uM)

C-constant concentration

COMBINATION I (SLIT2+ALW)	CI Values
IC	CI
30	8.04
50	2.06
70	1.06

B SW900 Isobologram of SLIT2-ensartinib combination

Legend:
- IC30
- IC50
- IC70
- SLIT2 C+ Ensartinib IC30
- SLIT2 C+Ensartinib IC50
- SLIT2 C+Ensartinib IC70
- SLIT2+ Ensartinib C IC30
- SLIT2+Ensartinib C IC50
- SLIT2+Ensartinib C IC70

Y-axis: SLIT2 concentration ug/ml
X-axis: Ensartinib concentration (uM)

COMBINATION I (SLIT2+ENSR)	CI Values
IC	CI
30	1.33
50	0.75
70	0.58

D SCC1 Isobologram of SLIT2-ensartinib combination

Legend:
- IC30
- IC50
- IC70
- SLIT2 C+ Ensartinib IC30
- SLIT2 C+Ensartinib IC50
- SLIT2 C+Ensartinib IC70
- SLIT2+ Ensartinib C IC30
- SLIT2+Ensartinib C IC50
- SLIT2+Ensartinib C IC70

Y-axis: SLIT2 concentration ug/ml
X-axis: Ensartinib concentration (uM)

C-constant concentration

COMBINATION I (SLIT2+ENSR)	CI Values
IC	CI
30	11.04
50	8.12
70	4.13

CI=COMBINATION INDEX	
CI>1 Antagonism	
CI=1 Additive effect	
CI<1 synergism	

E SW900 — Untreated, EphrinA1, SLIT2 (Cell proliferation vs Time (h)) ***

SCC1 — Untreated, EphrinA1, SLIT2 (Cell proliferation vs Time (h)) ***

G Alexa Flour 547-Red only | Alexa Flour 488-Green only
10μM

F SCC104 — Untreated, SLIT2, SLIT2+EGF (Cell proliferation vs Time (h)) ns ***

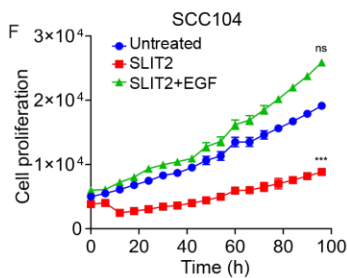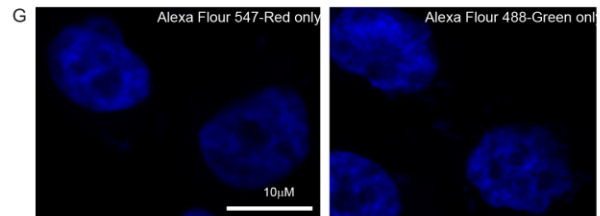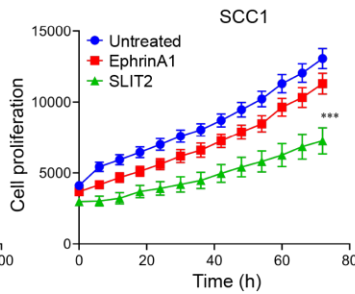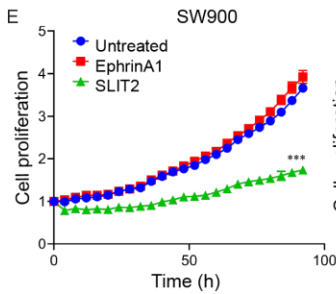SCC104 — Untreated, SLIT2, SLIT2+EGF (Caspase Activity vs Time (h)) ns **
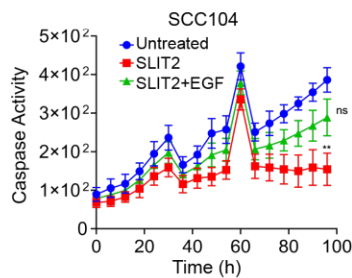
Fig S6

Supplementary tables

Supplementary table 2: Cell Lines. All HNSCC cell lines were obtained and validated by the following sources. HPV status of the following cell lines has been previously validated (Kimple RJ, 2013; Brenner J C, 2010). Related to Fig. 2.

Cell line	Sources	Culture condition
SCC-15 SCC-25	American Type Culture Collection	DMEM/F12 (1:1), 10% FBS, 400ng/ml, hydrocortisone, penicillin (100 units/mL), streptomycin (100 mg/mL)
93-vu-147T	Dr. Robert Ferris, with permission of Dr. Hans Joenje, VU Medical Center, Amsterdam, Netherlands	DMEM with 4.5 g/dL glucose, 10% FBS, penicillin (100 units/mL), streptomycin (100 mg/mL)
SCC4	DSMZ-German Collection of Microorganisms and Cell Cultures GmbH	
UD-SCC-2	Dr. Thomas Carey, with permission of Dr. Henning Bier, Technical University Munich, Munich, Germany	
UPCI: SCC-090	American Type Culture Collection	
TU-138	Dr. Jennifer Grandis, UCSF	DMEM/F12 (1:1)
HN30	Dr. Ravi Salgia, City of Hope	DMEM, 10% FBS, penicillin (100 units/mL), streptomycin (100 mg/mL) and NEAA
UM-SCC-1 UM-SCC-6	Millipore	EMEM medium supplemented with NEAA, 10% fetal bovine serum (FBS), penicillin (100 U/ml) and streptomycin (100 µg/ml)
SCC-1483	Dr. Lawrence Marnett, Vanderbilt University	DMEM with 4.5 g/dL glucose, 10% FBS, 1% hydrocortisone, penicillin (100 units/mL), streptomycin (100 mg/mL)
UM-SCC-47 UM-SCC-104 UM-SCC-22B	Millipore	

Supplementary table 3: Oligonucleotides List For: Forward Primer; Rev: Reverse Primer. Related to Fig. 1, 4 and 5.

shEPHA2#1 For	caccGCGTATCTTCATTGAGCTCAAtcaagagTTGAGCTCAATGAAGATACGC
shEPHA2#1 Rev	aaaaGCGTATCTTCATTGAGCTCAActcttgaTTGAGCTCAATGAAGATACGC
shEPHA2#2 For	caccTCGGACAGACATATAGGATATtcaagagATATCCTATATGTCTGTCCGA
shEPHA2#2 Rev	aaaaTCGGACAGACATATAGGATATctcttgaATATCCTATATGTCTGTCCGA
shROBO1 #1 For	caccGCAGAAATACAGTCACATTATtcaagagATAATGTGACTGTATTTCTGC
shROBO1#1 Rev	aaaaGCAGAAATACAGTCACATTATctcttgaATAATGTGACTGTATTTCTGC
shROBO1 #2 For	caccTGACACATGACGCCAGATAAtcaagagTTTATCTGGCGTCATGTGTCA
shROBO1 #2 Rev	aaaaTGACACATGACGCCAGATAAActcttgaTTTATCTGGCGTCATGTGTCA
EPHA2 coding For	aaaaactcgagATGGAGCTCCAGGCAGCCCGC
EPHA2 coding Rev	aaaaaggtaccGATGGGGATCCCCACAGTGTTCACC
ROBO1 coding For	ttttagatctATGATTGCGGAGCCCGCTCACTT
ROBO1 coding Rev	ttttcccgggcctgctgctgcGCTTTCAGTTTCCTCTAATTCTTCATTAT
ROBO1 FLAG Rev	ctagagtcgcggccgctTCACTTGTCGTCATCGTCTTTGTAGTCtgctgctgcGCTTTCAGTTTCC
EPHA2 HA Rev	atgatctagagtcgcggccgcTCAAGCGTAATCTGGAACATCGTATGGGTAtgctgctgcGATGGGG
EPHA2 K645R	CCGGTGGCCATCAGGACGCTGAAAGCCGG
ROBO1 Y932F	GAAGAGAAACGGACTTactagtACCttcGCGGGTATCAGAAAAGTAAC
ROBO1 Y1073F	ATCAGGGCAGCCTACTCCTttcGCCACCACTCAGCTCATC
vab-1 RNAi For	ttttggtaccGTTCTTGTTCCACGTGTCGTC
vab-1 RNAi Rev	tttagatctCCACATTCCACAAGTACATCC
sax-3 RNAi For	ttttggtaccTTCCGAAGTGAGTCTCTTCTC
sax-3 RNAi Rev	tttagatctCACCACCAACAATCGAGCATG
	For: Forward Rev: Reverse

Supplementary table 4: Antibodies List. Related to Fig. 1,2 and 5.

Antigen	Company	Cat#
FLAG Clone M2	Sigma	F1804
b-actin	Sigma	A5441
EPHA2	Santa Cruz	SC924
EPHA2 pS897	Cell signaling	6347
EPHA2 pY588	Cell signaling	12577
ROBO1	Invitrogen	PA5-29917
AKT pS473	Cell signaling	9271
EGFR pY1068	Cell signaling	2236

HA	Cell signaling	3724
ROBO1	Protein Tech	20219-1-AP

Transparent Methods

Cell Culture and Reagents

All NSCLC cell lines were from American Type Culture Collection (ATCC) (Manassas, VA, USA). NSCLC cell lines H2170, SK-MES-1, SW900 and the nonmalignant and immortalized control cell line BEAS-2B, were cultured in RPMI 1640 medium (Gibco/BRL) supplemented with 10% (v/v) fetal bovine serum (FBS), L-glutamine and 1% penicillin-streptomycin. HEK293 cells were cultured in DMEM medium (Gibco/BRL) supplemented with 10% (v/v) fetal bovine serum (FBS), L-glutamine and 1% penicillin-streptomycin. All HNSCC cell lines were obtained from indicated sources (**Supplementary Table 2**). All cell lines were cultured at 37°C with 5% CO_2. ALW-II-41-27 was purchased from MedChemExpress (Monmouth Junction, NJ, USA). ROBO1, EphrinA1, soluble EPHA2 and SLIT2 were purchased from R&D Systems (Minneapolis, MN, USA). EGF ligand was purchased from Stemcell Technology (Vancouver, Canada).

C. elegans RNAi and drug treatment

Culture and handling of *C. elegans* were carried out as described (Stiernagle, 2006). *vab-1* mutants (*OK1699, e2 and e2047*) and sax-3 mutants (*ky200 and ky123*) were obtained from *Caenorhabditis* Genetic Center. RNAi knockdown was carried out by bacterial feeding method (Kamath et al, 2001). Single wild type or mutant L3 worm were placed onto L4440 *E. coli* expressing either no RNA, or dsRNA targeting *vab-1* or *sax-3*. Total number of viable and dead F1 embryos were scored. For treatment with ALW-II-41-27, the indicated amount of drug or DMSO was added to 0.5 ml of base agar in 12-well plates and allowed to diffuse for 2 h. Feeding bacteria OP50 were then added on top of agar. A single L4 worm was then placed into an individual well. Viable F1 worms were then scored.

siRNA, shRNA, DNA vectors, transfection and cloning

shRNA plasmids were constructed by inserting annealed oligonucleotide pairs targeting EPHA2, ROBO1 or luciferase into pJR288 as described (Pang et al., 2018). The shRNA targeting EPHA2 and ROBO1 were transfected using jetPRIME® using manufacturer's protocol (Polyplus transfection, 67400 Illkirch, France). We used $2X10^5$ cells in a 6-well and transfected with 2µg of shRNA plasmid DNA. Transfection was done for indicated time points. Non-targeting control pool siRNA (catalog no. D-001810) and SMARTpool siRNA targeting EPHA2 (catalog no. L-003116) were purchased from Dharmacon, Inc. and were used at a final concentration of 15 nmol/L siRNA with Lipofectamine RNAiMAX (Life Technologies, Carlsbad, CA, USA). ROBO1 or EPHA2 expression vectors were

constructed by fusing PCR fragments containing full length ROBO1 or EPHA2 upstream to eGFP, mCherry, mClover3, mRuby3, HA or FLAG sequences. All expression vectors were based on peGFP-N3 (Clontech/Takara, Mountain View, CA, USA) with CMV promoter replaced by a eF1a promoter and eGFP replaced by mCherry, mClover3 or mRuby3. Point mutations were introduced by Q5 site directed mutagenesis kit according to manufacture protocol (New England Biolabs, Ispwich, MA, USA). All constructs were confirmed by DNA sequencing. Oligonucleotides used are listed in **Supplementary Table 3**.

Immunoblotting and immunoprecipitation

Cell lysates for immunoblotting were prepared by scraping cells and lysing them using RIPA buffer. Lysates were run on 4–15% or 4-20% Mini-protean TGX gels (Bio-Rad Laboratories, Hercules, CA, USA) and transferred onto Immobilon^{TM} membranes (MilliporeSigma, Burlingon, MA, USA) or Turboblot system (Bio-Rad). Blots were blocked using 5% nonfat dry milk in TBST for 1 h and incubated with primary antibodies (listed in **Supplementary Table 4**) overnight at 4°C. After washing 3 times in TBST, blots were incubated with HRP-conjugated secondary antibodies for 1 h at room temperature. The blots were then washed three times and immuno-reactive bands were detected by WesternBright ECL (Advansta, San Jose, CA, USA) or Azure Radiance (Azure) and imaged with ChemiDoc MP Imager (Bio-Rad) or Azure C600 (Azure). For co-immunoprecipitation assays, plasmids expressing EPHA2-HA and ROBO1-FLAG were cotransfected into HEK293 cells. Cells were collected 48 h post-transfection and lysed by IP buffer (PBS + 1% triton with HALT protease and phosphatase inhibitor cocktails) (ThermoFisher, Waltham, MA, USA). Lysates were adjusted to 1 mg/ml by IP buffer and protein complexes were immunoprecipitated by anti-FLAG magnetic beads (MilliporeSigma, Burlington, MA) or anti-HA magnetic beads (ThermoFisher) at 4^{0}C for 4 h. Immunoprecipitated complexes were detected by immunoblotting.

Cell viability assays

LSCC and HNSCC cells were labelled with m-Kate2 (red fluorescence) and stable cell lines were generated using puromycin selection. Labeled cells were seeded in 96 well plates for 24 h, followed by ligand treatment: SLIT2 (2μg/ml), EGF (0.5μg/ml) ensartinib and ALW-II-41-27 IC50 doses (**Table 4).** The caspase activity was monitored using Caspase green 3/7 reagent. Cells were imaged every 6 h for 96 h and their proliferation rates and caspase activity were plotted. Cell counting Kit 8 (Dojindo Molecular Technologies, catalog no. CK04) was used to determine relative numbers of viable cells 72 h after post transfection with shRNA targeting EPHA2 and ROBO1 in LSCC siRNA targeting EPHA2 (siEPHA2) and ROBO1 (siROBO1) in HNSCC.

Immunohistochemistry, immunofluorescence staining and live cells microscopy

Human lung cancer TMAs (LC642) were purchased from Biomax, Inc. (Rockville, MD, USA). EPHA2 was stained with anti-EPHA2 antibody (C-20, Santa Cruz Biotechnology, Dallas, TX, USA), 1:200 for 30 min, and ROBO1 was stained with anti-ROBO1 antibody

(PA5-29917, Invitrogen), 1:200 for 30 min. Each pair of stained TMAs was registered in Visiopharm before exporting a down sampled image. In FIJI, color deconvolution was used to extract the DAB staining (as grayscale) from each aligned TMA image, followed by pseudo-coloring the stains red or green. The staining was performed by the pathology/solid tumor core of The City of Hope National Medical Center. Each TMA was reviewed and scored by a pathologist on a scale of 0 to 3: 0+, no staining, no expression; 1+, weak staining, low expression; 2+, moderate staining, moderate expression; and 3+, strong staining, high expression. Scores of 0 and 1 were designated as low expression and scores of 2 and 3 were designated as high expression of EPHA2 or ROBO1. The resultant values of individual core for EPHA2 and ROBO1 scores were plotted as a pie chart using GraphPad Prism 7 software. (listed in **Supplementary Table 1**)

For immunofluorescence staining, cells were seeded in a Lab-Tek II Chamber Slide (ThermoFisher) or Number 1 cover slips in a 24-well plate for 24 to 48 h, then fixed by 1% formaldehyde in PBS for 20 min at room temperature, permeabilized by PBS containing 0.1% Tween and 0.25 % Triton X-100. After three washes with PBS, fixed cells were blocked with 5% FBS in PBS for 1 h at room temperature. Primary antibodies were then added and incubated overnight at 4^0C. Primary antibodies were removed, and the slides were washed 5 times with PBS. Alexa Flour 488 or Alexa Flour 547 conjugated secondary antibodies and Hoechst 33342 dye (ThermoFisher) or DAPI for staining nuclei were then added and allowed to incubate for 2 h at room temperature. The slides/coverslips were then washed five times with PBS and mounted in Prolong Gold Antifade reagent (ThermoFisher).

For live cell imaging, transfected cells were plated onto 35 mm Delta TPG dish (Bioptechs, Butler, PA, USA) for 24 h. The dishes were then placed on temperature controlled microscopic stage that was connected to CO_2 supply. All images were acquired on a Zeiss LSM880 confocal microscope and analyzed by Zen software (Zeiss USA, Thornwood, NY, USA).

Proximity Ligation Assay (PLA)

To perform a complete Duolink® PLA *in situ* experiment we used three primary antibodies (PLA, Immunofluorescence validated) that recognize EPHA2, ROBO1 or SLIT2 epitopes. The starter kit from SIGMA supplies all other necessary reagents for Duolink® PLA reactions, which include a pair of PLA probes (Anti-Rabbit PLUS and Anti-Mouse MINUS), red detection reagents, wash buffers, and mounting medium. The primary antibodies used came from the same species as the Duolink® PLA probes for EPHA2/ROBO1 or EPHA2/SLIT2 PLA (one mouse and one from rabbit species). Analysis was carried out using standard immunofluorescence assay technique. We used a confocal microscope (LSM880) to capture images. For the quantification of this staining the confocal images were extracted (multichannel to single channel), and a binary image was generated. The binary image was thresholded using FIJI software (Otsu). The average intensity was measured and plotted to compare the binding of the two proteins assayed.

Combination Index

For combination index (CI) calculation, LSCC (SW900) and HNSCC (SCC1) Incured cell lines were seeded in 96-well plate with 5000 cells per well. Three biological replicates (three 96-well plates for each drug combination) were used. For both cell lines, two drug combination were used SLIT2/ALW-II-41-27 and SLIT2-ensartinib. The drugs were used in linear dilution series with dilution factor of 2. SLIT2 doses ranged from $0\mu g/ml$-$6\mu g/ml$ and ALW-II-41-27 and ensartinib from $0\mu M$-$8\mu M$. The plates were read at 72 h using the IncuCyte Live Cell Analysis System to measure live cells (Incurred object count per well). We then use an R package called SynergyFinder (He et al., 2018) to find the nature of drug-drug interaction (i.e. if they work in synergy or antagonistically or non-interactively). For this purpose, the drug response matrix is supplied to the mentioned package, which then uses several models namely Highest Single Agent (Berenbaum, 1989), Loewe additivity (Loewe, 1953), Bliss independence (Bliss, 1939) and Zero Interaction Potency (Yadav et al., 2015) to quantify the degree of drug synergy. The dose response matrix was used to calculate individual CI values for IC30, IC50 and IC70 drug treatments. The output values were used to plot Isobolograms using the following formula.

$$CI = \frac{IC50\ (A)\ pair}{IC50\ (A)} + \frac{IC50\ (B)\ pair}{IC50\ (B)}$$

Statistical analysis

One-way ANOVA, non-linear regression or simple T-test were performed to calculate significance between data sets as indicated with each result or figure legend. A level of significance of $p < 0.05$ was chosen. Data are presented as mean with standard deviation of the mean ($\pm$ STD) in all figures in which error bars are shown. Graphs were generated using GraphPad Prism 7 software.

Supplemental References:

Berenbaum, M.C., 1989. What is synergy? Pharmacol. Rev. 41, 93–141.

Bliss, C.I., 1939. The toxicity of poisons applied jointly. Ann. Appl. Biol. 26, 585–615.

Brenner, J.C., Graham, M.P., Kumar, B., Saunders, L.M., Kupfer, R., Lyons, R.H., Bradford, C.R., Carey, T.E., 2010. Genotyping of 73 UM-SCC head and neck squamous cell carcinoma cell lines. Head Neck 32, 417–426.

He, L., Kulesskiy, E., Saarela, J., Turunen, L., Wennerberg, K., Aittokallio, T., Tang, J., 2018. Methods for high-throughput drug combination screening and synergy scoring. Methods Mol. Biol. 1711, 351–398.

Kimple, R.J., Smith, M.A., Blitzer, G.C., Torres, A.D., Martin, J.A., Yang, R.Z., Peet, C.R., Lorenz, L.D., Nickel, K.P., Klingelhutz, A.J., et al., 2013. Enhanced radiation sensitivity in HPV-positive head and neck cancer. Cancer Res. 73, 4791–4800.

Loewe, S., 1953. The problem of synergism and antagonism of combined drugs. Arzneimittelforschung 3, 285–290.

Pang, K.M., Castanotto, D., Li, H., Scherer, L., Rossi, J.J., 2018. Incorporation of aptamers in the terminal loop of shRNAs yields an effective and novel combinatorial targeting strategy. Nucleic Acids Res. 46, e6.

Stiernagle, T. (2006). Maintenance of C. elegans. Worm Book the Online Review of C. elegans Biology. WormBook Research Community.

Yadav, B., Wennerberg, K., Aittokallio, T., Tang, J., 2015. Searching for drug synergy in complex dose-response landscapes using an interaction potency model. Comput. Struct. Biotech. J. 13, 504–513.